



# UNIVERSITAT DE BARCELONA

Final Degree Project  
**Biomedical Engineering Degree**

**“Study of a medical device to treat  
aortic dissection with Finite Element  
Analysis “**

Barcelona, 7th June 2023

Author: Alba Casero Sánchez

Director/s: Eduardo Soudah Prieto

Tutor: Manuel Carmona Flores

## Acknowledgments

I would like to express my appreciation and gratitude to my project director, Eduardo Soudah Prieto, and my tutor, Manuel Carmona Flores, for their guidance, support, and expertise throughout the duration of this project. Their contributions have been crucial for the successful completion of this project and have expanded my knowledge in the topic and enriched my learning experience.

First, I would like to thank Eduardo Soudah Prieto for the time and effort he invested into mentoring me, providing me with insightful feedback, helping me to overcome the problems encountered, and guiding me during the whole process.

I am also very grateful to Manuel Carmona Flores for his help in the second part of the project. His extensive knowledge and expertise in Elmer were very valuable and without his help this project wouldn't have been possible. I would like to thank him for his commitment and dedication to work for the success of the project and his help and support every time I faced a problem.

Finally, I would like to thank my family and friends for their unconditional support, always cheering me up when I faced an obstacle.

## Abstract

The aortic dissection is a cardiovascular disease that results from the rupture of the inner layer of the aorta. Type B aortic dissections commonly become a chronic disease with a high long-term morbidity and mortality rates. Current treatments include open surgery repair and thoracic endovascular aortic repair (TEVAR). However, new non-invasive treatments are being developed that favour the own regeneration of the tissue, avoiding the permanent presence of a foreign device in the body.

This project focuses on the understanding of a new treatment with a medical device, an aortic patch, by *in silico* testing. The goal is to determine the performance of the patch in a simulated aortic dissection and then compare it with the current treatment with the stent graft (TEVAR), to determine if it would avoid the hypertension that can be caused by the stent. To do the first part, it was created a model of the aortic dissection, but due to complications with the simulation, this part of the project couldn't be finished, and the performance of the patch in the aortic dissection couldn't be determined. To do the second part three models were created: healthy aorta, aortic dissection with stent graft and aortic dissection with patch. A transient simulation was run for the three models and the pressure waveform was analyzed.

The results show that the pressure in the stent graft model is higher, and the patch has a similar response to the healthy aorta. However, all the models presented hypertension (including the healthy aorta) and the differences between the models are too small to be concluding, so it cannot be assured that the patch is a better option than the stent graft to avoid causing hypertension in the aortic dissection treatment.

**Keywords:** aortic dissection, medical device, aortic patch, stent graft, FSI, open source

## LIST OF FIGURES

<b>Figure 1.</b> Aortic dissection pathophysiology. Extracted from [2].	3
<b>Figure 2.</b> Aortic dissection classification. Extracted from [3].	3
<b>Figure 3.</b> Healthy aorta model [own source].	28
<b>Figure 4.</b> Healthy aorta STL model with mesh element size of 0.5 [own source].	28
<b>Figure 5.</b> Healthy aorta STL model with mesh element size of 0.1 [own source].	29
<b>Figure 6.</b> Model section of the pipeline in SimVascular [own source].	29
<b>Figure 7.</b> Mesh section of the pipeline in SimVascular [own source].	30
<b>Figure 8.</b> Properties of the aortic wall in the deformable model in CGS units [own source].	31
<b>Figure 9.</b> Plot over line process in the results of the first simulation [own source].	32
<b>Figure 10.</b> Aortic dissection model [own source].	33
<b>Figure 11.</b> Model faces identification in SimVascular [own source].	33
<b>Figure 12.</b> Sketches of the models to be designed [own source].	34
<b>Figure 13.</b> Endovascular stent graft for aortic dissection. Extracted from [52].	34
<b>Figure 14.</b> Mesh generation in GMSH [own source].	35
<b>Figure 15.</b> Meshed model of the healthy aorta (A), aorta with stent graft (B), and aorta with patch (C) [own source].	36
<b>Figure 16.</b> Set up of the simulation [own source].	37
<b>Figure 17.</b> Blood equations (Navier-Stokes and Mesh Update) [own source].	38
<b>Figure 18.</b> Aortic wall equation (Nonlinear elasticity) [own source].	38
<b>Figure 19.</b> Solver Settings of the Navier-Stokes [own source].	39
<b>Figure 20.</b> Solver settings of the non-linear elasticity [own source].	39
<b>Figure 21.</b> Initial conditions [own source].	40
<b>Figure 22.</b> Axisymmetry boundary condition [own source].	41
<b>Figure 23.</b> FSI boundary condition [own source].	41
<b>Figure 24.</b> Clamp boundary condition [own source].	42
<b>Figure 25.</b> Pressure at the outlet in the study of Zorrilla et al. Extracted from [1].	42
<b>Figure 26.</b> Pressure at the outlet in Elmer [own source].	42
<b>Figure 27.</b> Velocity at the inlet in the study of Pavel et al. Extracted from [15].	43
<b>Figure 28.</b> Velocity imposed at the inlet in Elmer [own source].	43
<b>Figure 29.</b> Pressure distribution of the first simulation [own source].	45
<b>Figure 30.</b> Pressure distribution of the second simulation [own source].	46
<b>Figure 31.</b> Pressure distribution of the third simulation [own source].	47
<b>Figure 32.</b> Displacement in the deformable model (units: cm) [own source].	48
<b>Figure 33.</b> Hydrodynamic entrance length. Extracted from [58].	49
<b>Figure 34.</b> Proximal pressure waveform of the simulated healthy aorta [own source].	51
<b>Figure 35.</b> Reference pressure waveform of the healthy aorta. Extracted from [62].	51
<b>Figure 36.</b> Displacement of the healthy aortic wall (units: m) [own source].	51
<b>Figure 37.</b> Proximal pressure waveform of the aortic dissection with the stent graft [own source].	53
<b>Figure 38.</b> Proximal pressure waveform of the aortic dissection with the patch [own source].	54
<b>Figure 39.</b> Work-breakdown structure of the project [own source].	55
<b>Figure 40.</b> Gantt chart of the project [own source].	56

## LIST OF TABLES

<b>Table 1.</b> Specific objectives for Part I and Part II of the project. ....	1
<b>Table 2.</b> State of the art in aortic dissection FEM simulation studies.....	21
<b>Table 3.</b> Studied solutions for the project. ....	23
<b>Table 4.</b> Solutions proposed for the first part of the project. ....	26
<b>Table 5.</b> Solutions proposed for the second part of the project. ....	27
<b>Table 6.</b> SimVascular basic parameters. ....	30
<b>Table 7.</b> Flow imposed at the inlet in SimVascular. ....	30
<b>Table 8.</b> RCR values employed in SimVascular in CGS units. ....	31
<b>Table 9.</b> Solver parameters introduced in SimVascular.....	31
<b>Table 10.</b> Material properties. ....	39
<b>Table 11.</b> SWOT analysis of the project. ....	57
<b>Table 12.</b> Breakdown of the estimated costs of the project. ....	59

## LIST OF ABBREVIATIONS

<b>2D PC-MRI</b>	Two-dimensional phase contrast MRI
<b>4D PC-MRI</b>	Four-dimensional phase-contrast MRI
<b>AD</b>	Aortic dissection
<b>CT</b>	Computed tomography
<b>CAD</b>	Computer-aided design
<b>CFD</b>	Computational fluid dynamics
<b>CIMNE</b>	Centre for Numerical Methods in Engineering
<b>CMR</b>	Cardiovascular magnetic resonance
<b>CTA</b>	Computed tomography angiography
<b>EMA</b>	European Medicines Agency
<b>FL</b>	False lumen
<b>FDA</b>	Food and Drug Administration
<b>FEA</b>	Finite element analysis
<b>FEM</b>	Finite element method
<b>FL <math>\Delta P_{\max}</math></b>	False lumen relative pressure
<b>FLEF</b>	False lumen ejection fraction
<b>FSI</b>	Fluid-structure interaction
<b>GUI</b>	Graphical user interface
<b>IF</b>	Intimal flap
<b>MSDR</b>	Maximum systolic deceleration rate
<b>OSI</b>	Oscillatory shear index
<b>OSR</b>	Open surgical repair
<b>PC-MRI</b>	Phase-contrast magnetic resonance imaging
<b>PDTSR</b>	Proximal and distal tear size ratio
<b>TL</b>	True lumen
<b>TAAD</b>	Type A aortic dissection
<b>TBAD</b>	Type B aortic dissection
<b>TEVAR</b>	Thoracic endovascular aortic repair
<b>UB</b>	University of Barcelona
<b>UPC</b>	Polytechnic University of Catalonia
<b>WSS</b>	Wall shear stress

## Table of contents

1. Introduction .....	1
1.1- Objectives .....	1
1.2- Scope and limitations .....	1
1.3- Location of the project .....	2
2. Background .....	3
2.1- General concepts .....	3
2.1.1- Aortic dissection .....	3
2.1.2- FDA and <i>in silico</i> models .....	5
2.2- State of the art .....	6
3. Market analysis .....	22
4. Conception engineering .....	23
4.1- Solutions studied .....	23
4.1.1- Modelling software .....	23
4.1.2- Meshing software .....	24
4.1.3- Simulation software .....	24
4.1.4- Post-processing software .....	25
4.2- Solution proposed .....	25
4.2.1- Part I .....	26
4.2.2- Part II .....	27
5. Detail engineering .....	28
5.1- Part I .....	28
5.1.1- Healthy aorta .....	28
5.1.2- Aortic dissection .....	32
5.2- Part II .....	34
5.2.1- Modelling .....	34
5.2.2- Meshing .....	35
5.2.3- Simulation .....	36
5.2.4- Post-processing .....	44
5.3- Results and discussion .....	44
5.3.1- Part I .....	44
5.3.2- Part II .....	50
6. Execution chronogram .....	54
6.1- Work-breakdown structure (WBS) .....	54

6.2- Gantt chart.....	55
7. Technical viability.....	57
7.1- Strengths .....	57
7.2- Weaknesses .....	57
7.3- Opportunities .....	58
7.4- Threats .....	58
8. Economic viability .....	59
9. Regulation and legal aspects .....	60
10. Conclusions .....	62
11. References.....	63



# 1. Introduction

## 1.1- Objectives

The main goal of this project is to determine the hemodynamic performance of a medical device to treat type B aortic dissection. It is a biomimetic resorbable patch that, using an endovascular catheter, is placed on the aortic tear, stopping the false lumen blood flow, and promoting the natural repair and bio-integration.

The project has been divided into two different parts. In the first one, the aim is to determine how much does the aortic dissection improve with the patch. In the second one, the aim is to compare the patch with the current treatment, the stent graft, and determine if the patch would be better to avoid the hypertension that can be caused by the stent.

For the two parts of the project some specific objectives were proposed. These ones are shown in Table 1.

**Table 1.** Specific objectives for Part I and Part II of the project.

Part I	Part II
Familiarise with the GiD and SimVascular software.	Familiarise with the Gmsh and Elmer software.
Test SimVascular with one of the example projects provided to ensure that the expected results are obtained.	Make the 3 models: healthy aorta, aortic dissection with the stent graft, and aortic dissection with the patch.
Make the 3 models: healthy aorta, aortic dissection, and aortic dissection with the patch.	Determine which is the optimal mesh for each model (number of elements in the fluid and the wall).
Select the best mesh element size for the 3 models.	Perform fluid-structure interaction simulations with the 3 models.
Perform fluid-structure interaction simulations with the 3 models.	

## 1.2- Scope and limitations

As mentioned before, the objective of this project is to understand the mechanics of the new treatment (aortic patch) for aortic dissection and assess its impact, compared with the aortic dissection without it and the aortic dissection with the stent graft, having as a reference what is the behaviour of the healthy aorta. Due to the limited time to do the project, the simulations couldn't be performed with patient-specific models, so the scope of the project was to model and simulate ideal models, simplifying the geometry of the aorta as a cylinder with the corresponding dimensions.

During the project, different limitations were faced. To carry out the first part of the project, the author had to use a software (SimVascular) with no prior knowledge. In addition, there wasn't much information on the internet about this program, apart from the tutorials offered by the same software webpage. There was a forum in which the creators tried to troubleshoot the problems of the users, but the information given was not always enough or didn't help much.

Several problems were found with SimVascular, starting with the solver, as the fluid-structure interaction (FSI) solver needed to perform non-linear elastic simulations was not available for Windows, that is the only operating system that the author had. Therefore, the only option was to make FSI simulations with the coupled momentum method, which considers a thin linear elastic membrane, so it doesn't correctly represent the reality. Another limitation faced was that when importing the aortic dissection model, the faces weren't correctly identified, and the mesh couldn't be correctly generated. In addition, it wasn't found any way to define different domains in the model with SimVascular, which was essential for a correct simulation. It is important to remark that the decision to choose SimVascular was based on the analysis of the state of the art because it seemed a promising software for this application. However, these unexpected limitations were found during the process, which made that this part of the project couldn't be continued. As a result, it was decided to change the focus of the project and make a study with another software (Elmer) comparing the patch with the stent graft instead of comparing it with the aortic dissection, that is the model that generated problems.

Finally, as Elmer is not a software designed for biomechanical finite element method (FEM) simulations, complex simulations could not be performed. There was just a model to perform non-linear simulations so it could not be solved using the Holzapfel-Gasser-Ogden hyperelastic model, that is the one that better describes the behaviour of the aorta. Moreover, in the output, the three-element Windkessel model boundary condition could not be applied because it was not available in Elmer, so instead a single resistance was imposed at the output.

### 1.3- Location of the project

The project has been developed in collaboration with the University of Barcelona (UB) and the Bio-Medical Engineering group of the International Centre for Numerical Methods in Engineering (CIMNE), which is a public R+D centre in computational engineering located in the Campus Nord of the Polytechnic University of Catalonia (UPC). The project was supervised by Eduardo Soudah Prieto, associate professor at UPC and group leader of the Bio-Medical Engineering group, and tutored by Manuel Carmona Flores, associate professor at UB. The project was mainly performed tele-working with the help of weekly virtual meetings with the supervisor and weekly face-to-face meetings with the tutor for the second part of the project.

## 2. Background

### 2.1- General concepts

#### 2.1.1- Aortic dissection

The aortic dissection (AD) is a cardiovascular disease that results from the rupture of the inner layer of the aorta. The blood flowing through the opened space (tear) causes the inner and middle layers of the aorta to split/dissect (Figure 1). The normal lumen of the aorta is referred as true lumen (TL) and the dissected lumen as false lumen (FL). The wall shared between both is the intimal flap (IF) [1].

It is a very severe pathology and becomes fatal when the blood goes through the outer aortic wall. There are two types of aortic dissection depending on their location. Ascending ADs or type A are those located in the ascending region of the aorta or the aortic arch, whereas descending ADs or type B are those located in the descending region of the aorta (Figure 2). Type A ADs can be usually treated through surgical interventions, while type B ADs commonly become a chronic disease with a high long-term morbidity and mortality rates. The survival rate is around 50-80% after 5 years and decreases to 30-60% after 10 years. This is due to the progressive dilation of the AD, which can be due to the number, location and size of the intimal tears, the elasticity of the IF, the pressure difference between the TL and FL or the high intraluminal pressure that can result in the rupture of the aortic wall. It is crucial to identify the pressure peaks and locate the points of the dissection tears to prevent lethal outcomes and numerical simulation can play an important role assessing the hemodynamics of the AD and simulate real patient-specific scenarios [1].

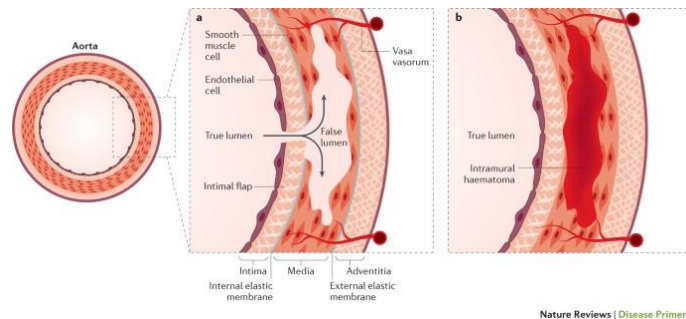


**Figure 1.** Aortic dissection pathophysiology. Extracted from [2].

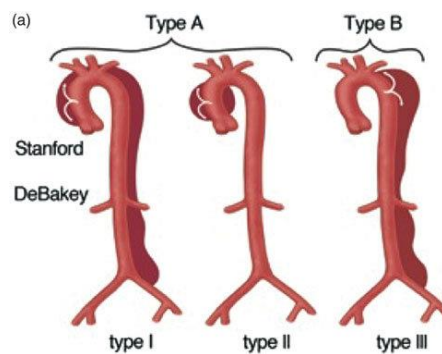


**Figure 2.** Aortic dissection classification. Extracted from [3].

#### 4D MRI diagnosis

Computed tomography angiography (CTA) is the most widely used diagnostic method for patients with acute aortic pathology as it is a rapid imaging technique, and it is less invasive than conventional aortography. However, CTA still requires the use of contrast media and radiation [4].

MRI is a non-invasive imaging technique that is widely used to evaluate cardiovascular diseases based on both anatomical and functional information. The past decades have seen the rise of two-dimensional phase contrast MRI (2D PC-MRI) for blood flow quantification. It was originally described in the 1980s and takes advantage of the direct relationship between blood flow velocity and phase of the MRI signal. More recently, it was developed the imaging technique of four-dimensional phase-contrast MRI (4D PC-MRI), which can measure the aorta blood flow velocity in any direction, and by calculating the blood flow volume and flow pattern is possible to make a functional assessment of the blood flow. With the resulting data (3D + time + 3 velocity directions) several derived fluid mechanics parameters can be calculated, such as wall shear stress (WSS), kinetic energy and pressure gradients. This technique offers the opportunity to better understand and assess *in vivo* 3D blood flow dynamics. For this reason, there is intensive research going on in the field [5].

#### Treatments

Patients with chronic type B aortic dissection (TBAD) can be classified as being complicated TBAD or uncomplicated TBAD. Uncomplicated TBAD can be treated with optimal medical therapy, which usually consists of the administration of beta-blockers to decrease arterial blood pressure or, alternatively, calcium channel blockers can be used [6, 7]. On the other hand, complicated TBAD usually need to be treated with surgery, that can be either thoracic endovascular aortic repair (TEVAR) or open surgical repair (OSR). However, for the treatment of ischemic complications of the aortic dissection it is performed the procedure of surgical aortic fenestration, which consists of making a puncture of the IF from the TL to the FL using a needle. This technique is less invasive than TEVAR and it corrects the malperfusion at the suprarenal or infrarenal levels by creating a single aortic lumen to restore organ flow. The creation of the new reentry tear in the distal part of the IF can also be used to decompress the hypertensive false lumen [1].

#### Open surgical repair

For many years, OSR was the only treatment option for people with chronic TBAD. The aim of this treatment is to replace the site of the primary intimal tear with a synthetic graft. After the occlusion of proximal and distal tears, the aorta is opened longitudinally, thrombi are removed from the false lumen and the true lumen is entered. Then the orifices of the segmental arteries and oesophageal or bronchial arteries above the level of the sixth intercostal space are ligated. Finally, the aorta is completely transected and the corresponding proximal and distal grafts are reinforced. This approach, however, presents some complications such as renal failure (8.1%), spinal cord ischemia (4.9%), reintervention for bleeding (8.1%), and early mortality (8.3%) [8].

## Thoracic endovascular aortic repair

Endovascular repair was introduced after OSR and nowadays is considered by some to be a better treatment option as it is much less invasive. A preoperative CTA must be performed to evaluate the level of calcification, the patency, and the perfusion of the FL, as well as the number of thrombi present and the chronicity of the septum. To perform the surgery, sheaths are used to access femoral or brachial arteries and then catheters and guidewires are used to access the thoracic aorta under fluoroscopic guidance. The endograft is advanced to, and deployed in, the thoracic aorta. There are also some challenges concerning this type of treatment. For example, the size of the TL and the stiffness of the intraluminal septum because if the lumen is too narrow and the septum is too stiff, the endograft can have difficulties to expand. Another possible complication is the arise of visceral branches from the TL or FL. In the last case, stenting may be needed to maintain perfusion once the FL has been excluded. If the FL is aneurysmal and is not completely thrombosed, it may be required to induce thrombosis to prevent further aneurysm expansion [8].

### 2.1.2- FDA and *in silico* models

Computational (*in silico*) modelling and simulation is used to complement *in vitro* testing, animal studies and clinical trials. The modelling and simulation studies applied to healthcare are reviewed by the Food and Drug Administration (FDA), in the United States, or the European Medicines Agency (EMA), in the European Union [9].

The use of computational modelling techniques like computational fluid dynamics (CFD) and finite element analysis (FEA) can help to improve the design and testing of medical devices such as cardiovascular stents that are implanted in the human body. Flow-visualization and CFD simulations can be used to validate and predict blood damage [10]. CFD uses numerical methods and algorithms to solve and analyse problems that involved fluid flows [11, 12, 13]. It is one of the most widely used computational modelling techniques and it has already been used for testing of blood-flow medical devices, such as ventricular assisted devices. Another computer modelling technique used is FEA, which predicts the stresses and strains in solid materials from the applied external forces and deformations by knowing the geometry and the mechanical properties of the device [14]. In cardiovascular applications, it is becoming more popular de use of fluid-structure interaction (FSI) simulations, which are a coupled CFD and FEA cases.

The advantage of these methods is that they could replace or augment clinical trials with *in silico* clinical trials. A virtual cohort of patients could be used to evaluate medical products when real clinical trials would be unethical. Moreover, it could be used to augment and potentially reduce the required size of clinical trials, or to even replace clinical trials. This can also be extended to animal studies, so that with *in silico* simulations less animal testing is needed, decreasing animal torment during experimental studies and reducing the number of animals killed every year. In addition, *in silico* studies would reduce costs because with a virtual model there is no need to build and test the device prototypes. However, there is still lack of standardization protocols in this type of studies so further validation is required [9, 14].

## 2.2- State of the art

**Title:** Computational modelling of the fluid flow and the flexible intimal flap in type B aortic dissection via a monolithic arbitrary Lagrangian/Eulerian fluid-structure interaction model.

**Reference:** [15]

**Year:** 2019

**Summary:** In the present work FSI simulations of the fluid flow in type B aortic dissection are performed, accounting for the flexibility of the intimal flap. The numerical results show good agreement with the experimental evidence and the previously published numerical simulations. The numerical model (FSI) is capable of capturing the complex flow patterns generated by the flexible IF, including the formation of recirculation zones, stagnation points and vortices at the vicinity of the tear. The numerical simulations show that the tear size has a significant influence on the fluid flow and on the flap deformation. The flap deformation is higher for the larger tear size, leading to the formation of a larger recirculation zone and higher pressure drops. The results suggest that the flexible IF plays an important role in the fluid flow in type B AD, and that the tear size has a significant influence on the flow and the flap deformation.

**Segmentation/Program used/Phantom or real:** Geometrical model obtained from [2]. Different configurations of tear positions/sizes were studied.

**Simulation/Code used/Type of simulation:** KRATOS (open-source simulation code developed by CIMNE). FSI simulation. 3D meshing using GiD.

### **Boundary conditions:**

**Inlet:** Parabolic profile (formula) to impose a parabola in the inlet. Velocity is time dependent obtained from the experiment [16].

**Outlet:** Data measured in the experiment [16] (time dependent).

**Wall (material):** Young's modulus:  $E=1.07$  MPa, Poisson's ration:  $\nu=0.4$ , Density:  $\rho=2000$ kg/m<sup>3</sup>.

**Blood density:** 1000 kg/m<sup>3</sup>.

**Blood viscosity:**  $0.86 \times 10^{-6}$  m<sup>2</sup>/s.

**Title:** Validation of numerical flow simulations against *in vitro* phantom measurements in different type B aortic dissection scenarios.

**Reference:** [16]

**Year:** 2015

**Summary:** The aim of this study is to validate a CFD tool for hemodynamic chronic type B aortic dissection. The numerical results were validated for different dissection geometries with experimental data obtained from a previous *in vitro* study performed on idealized dissected physical models. The results obtained with the CFD simulations showed good correlation with the experimental measurements if the tear size was large enough to neglect the effect of the wall compliance.

**Segmentation/Program used/Phantom or real:** Ideal model (phantom). TL diameter of 14mm, dissected segment diameter of 40mm, FL length of 160mm, dissection flap thickness of 2mm and TL length of 390mm. Centres of proximal and distal tears located at 175.5mm and 320.5mm from the inlet, respectively. Tear diameters of 4mm or 10mm, different cases studied.

**Simulation/Code used/Type of simulation:** GiD to construct the meshes, Tdyn (CompassIS, Barcelona, Spain) for the CFD simulation.

**Boundary conditions:**

**Inlet:** Time-dependent parabolic velocity profile. Velocity is obtained from *in vitro* experiments.

**Outlet:** Time-dependent pressure waveform obtained from *in vitro* experiments.

**Wall (material):** Aortic wall assumed to be rigid.

**Blood density:** 996 Kg/m<sup>3</sup>.

**Viscosity:**  $0.86 \cdot 10^{-3}$  Kg/(ms).

**Title:** Fluid–structure interaction simulations of patient-specific aortic dissection.

**Reference:** [17]

**Year:** 2020

**Summary:** A FSI numerical model for CFD simulations of aortic dissection is presented, capturing the complexity interplay between physiologic deformation, flow, pressures, and time-averaged WSS in a patient-specific model. The simulations closely capture the cyclical deformation of the dissection membrane, with flow simulations similar to 4D flow MRI. It is demonstrated that decreasing the flap stiffness from 800kPa to 20kPa increases the displacement of the dissection flap from 1.4mm to 13.4mm, decreases the surface area of time-averaged WSS by a factor of 2.3, decreases the mean pressure difference between the TL and FL by a factor of 0.63, and decreases the TL flow rate by up to 20% in the abdominal aorta. It is concluded that the mobility of the dissection flap affects local hemodynamics and therefore has to be considered for patient-specific simulations of aortic dissection.

**Segmentation/Program used/Phantom or real:** Real model (CTA), and 4D flow MRI. CTA is used to obtain the geometrical model. Image segmentation and model generation were performed in SimVascular (Updegrove et al. 2016), an open-source patient-specific cardiovascular flow modelling software, with supplemental editing performed in Meshmixer (Autodesk, Inc.).

**Simulation/Code used/Type of simulation:** The proposed computational framework consists of (1) two-way FSI simulations using an arbitrary Lagrangian–Eulerian formulation to account for tissue deformation; (2) prestress of the arterial wall and (3) tissue support of the structural domain to avoid unphysiologic dilation of the aortic wall and stretching of the dissection flap; (4) tethering of the aorta to restrict translatory motion of the aorta; and (5) independently defined elastic modulus for the dissection flap and the outer vessel wall to account for their different material properties. The numerical simulations are performed with the svFSI finite element solver from the SimVascular package. The meshing is generated using TesGen. A description of the mesh generation can also be found at <http://simvascular.github.io/docssvFSI.html>

**Boundary conditions:**

**Inlet:** Time-dependent Dirichlet condition with a given velocity  $v_{in}$ . The inlet flow rate is obtained from the 4D flow MRI. Nodal values at the inlet surface are determined by assuming a parabolic cross-sectional profile.

**Outlet:** Three-element Windkessel boundary conditions, according to the coupled multidomain method as described in Esmaily-Moghadam et al. (2013).

**Wall (material):** Arterial tissue is generally considered incompressible (Holzapfel 2000). However, in the current framework the tissue is modelled as nearly incompressible by setting the Poisson ratio  $\nu = 0.49$  in the whole structural domain. The Young's modulus in the wall is 800kPa and the Young's modulus in the IF has been varied in every run, taking the following values: 20kPa, 50kPa, 100kPa and 800kPa.

**Flap thickness:** 2mm.

**Blood density:** 1060 kg/m<sup>3</sup>.

**Blood viscosity:** 0.004 Pa·s.



**Title:** Fluid-Structure Interaction Simulations of Repaired Type A Aortic Dissection: a Comprehensive Comparison With Rigid Wall Models.

**Reference:** [18]

**Year:** 2022

**Summary:** The aim is to evaluate the effect of aortic wall compliance on intraluminal hemodynamics within surgically repaired type A aortic dissection (TAAD). FSI simulations were performed to patient-specific post-surgery TAAD models reconstructed CTA images. Computational results were compared between the FSI and rigid wall simulations. It was found that the FSI model predicted lower blood velocities and WSS along the dissected aorta. FSI models produced more turbulent flow, where much larger regions presented higher turbulent intensity in comparison to rigid models. The effect of wall compliance on pressure difference between the TL and FL was similar between both models (FSI and rigid). Simulations with different Young's moduli were performed and the results showed that a more compliant wall was translated into a velocity and WSS reduction because of increased displacements. In conclusion, FSI can more accurately predict the low WSS regions in surgically repaired TAAD, but rigid wall models are enough to predict luminal pressure difference.

**Segmentation/Program used/Phantom or real:** A real model is used. The geometrical model is obtained from CTA images using Mimics 20.0 (Materialise, Leuven, Belgium). Fluid and solid domains were meshed using ANSYS ICEM CFD 19.2 (ANSYS, Canonsburg, PA, United States).

**Simulation/Code used/Type of simulation:** The wall models were solved using ANSYS Transient Structure solver, while the pulsatile blood flow was solved using ANSYS CFX 19.2. The two-way FSI simulation was then performed using ANSYS system coupling (ANSYS, Canonsburg, PA, United States), which couples ANSYS Structure and ANSYS CFX through a partitioned approach.

**Boundary conditions:**

**Inlet:** Scaled patient-specific flow waveform assuming a flat velocity profile.

**Outlet:** Three-element Windkessel model.

**Wall (material):** A Young's modulus of 1.3 MPa was imposed for the aortic dissected wall and IF. Additional FSI simulations were run with different Young's moduli (1.08 and 2 MPa) to assess the impact of aortic stiffness in the predicted results. The Dacron graft used to replace the ascending aorta is made of polyethylene terephthalate, with a Poisson's ratio of 0.3 and a Young's modulus of 7.8 MPa [19].

**Blood density:** 1060 Kg/m<sup>3</sup>.

**Viscosity:** 0.004 Pa·s.

**Title:** Aortic dissection assessment by 4D phase-contrast MRI with hemodynamic parameters: the impact of stent type.

**Reference:** [4]

**Year:** 2021

**Summary:** The aim of the study is to explore the diagnostic performance of 4D PC-MRI in evaluating aortic dissection in different clinical scenarios. The study comprised 32 patients who underwent CTA and 4D PC-MRI. The 4D PC-MRI images were then compared with the CTA images. Patients were divided into three groups: (I) patients diagnosed with TBAD that did not undergo intervention (n=8), (II) patients with residual aortic dissection after open repair of TAAD (n=7), (III) patients who underwent endovascular aortic repair with or without open surgery (n=7). 4D PC-MRI provided similar aortic images for patients in group 1 and most in group 2. In group 3 stainless steel stents affected image quality in three patients, whereas in the rest of the patients (with non-stainless-steel stents) high-quality images were obtained. Not only were provided images of comparable quality to those obtained with CTA but also information on hemodynamic parameters, including endoleak detection after thoracic endovascular repair. Therefore, 4D PC-MRI shows great potential for the diagnosis of aortic dissection, except for those cases with stainless steel materials.

**Image acquisition:** CTA and 4D PC-MRI with a 1.5-T MR scanner (Ingenia Rev R5 V30-rev.02; Philips, Amsterdam, The Netherlands).

**Title:** False lumen pressure estimation in type B aortic dissection using 4D flow cardiovascular magnetic resonance: comparisons with aortic growth.

**Reference:** [20]

**Year:** 2021

**Summary:** The aim is to investigate the association between aortic growth and three cardiovascular magnetic resonance (CMR)-derived metrics of FL pressurization: FL ejection fraction (FLEF), maximum systolic deceleration rate (MSDR), and FL relative pressure (FL  $\Delta P_{\max}$ ). CMR was performed in 12 patients, including contrast enhanced CMR and 4D flow CMR. FLEF was higher in enlarging chronic TBAD, whereas FL  $\Delta P_{\max}$  was lower. MSDR and conventional anatomic variables did not differ significantly between groups. FLEF showed positive correlation with aortic growth rate whereas FL  $\Delta P_{\max}$  showed negative correlation. These results suggest that 4D flow CMR derived metrics of FL pressurization can be useful to separate patients at highest and lowest risk for progressive aortic growth and complications.

**Image acquisition:** CMR exams were performed on 3T scanners (n = 1: MR750, General Electric Healthcare, Milwaukee, Wisconsin, USA; n = 11: Ingenia, Philips Healthcare, Best, The Netherlands). The CMR examination included contrast-enhanced magnetic resonance angiography and 4D flow CMR.

**Segmentation:** Segmentations were generated with Mimics (Materialise, Leuven, Belgium) on CE-MRA images. Once the segmentations were done, an inhouse MATLAB (MathWorks, Natick, Massachusetts, USA) toolbox was used to perform a range of image processing steps. The software Arterys (San Francisco, California, USA) was used for data reconstruction (from 4D flow CMR DICOM data), visualization and flow analysis.

**Title:** Advanced risk prediction for aortic dissection patients using imaging-based computational flow analysis.

**Reference:** [21]

**Year:** 2022

**Summary:** This paper presents a review on the application of imaged-based CFD simulations and 4D-flow MRI analysis for risk prediction in aortic dissection. Finally, it is proposed a workflow incorporating computational modelling for personalized assessment to aid in risk stratification and treatment decision-making.

**Segmentation/Program used/Phantom or real:** Patient-specific geometry is commonly reconstructed from contrast-enhanced CTA images. For the mesh generation, an unstructured mesh containing tetrahedral elements in the core and prism elements in the near wall region is widely adopted for AD models.

**Boundary Conditions:**

**Inlet:** The optimal inlet boundary condition is a patients-specific velocity profile obtained from *in vivo* measurements, using non-invasive techniques such as MRI or Doppler ultrasound; however, obtaining this information is not always possible, so in this case generic flow waveforms along with the assumption of flat, parabolic, or Womersley velocity profiles are often adopted.

**Outlet:** A suitable outlet boundary condition can be specified using the three-element Windkessel model, which describes the arterial system by characterising the arterial compliance ( $C$ ), the peripheral resistance ( $R_p$ ), the total impedance of the aorta ( $R_c$ ).

**Wall (material):** In FSI models the wall is compliant whereas in rigid wall models is rigid (ideal model). FSI simulations provide more accurate results, but they have excessive computational costs.

**Title:** Computational modelling of the fluid flow in type B aortic dissection using a modified finite element embedded formulation.

**Reference:** [1]

**Year:** 2020

**Summary:** The aim of this study is to explore the use of an embedded CFD method to investigate the type B aortic dissection. The correctness and suitability of the presented approach is proven by comparing the pressure values and waveform with the measurements obtained in an *in vitro* experiment present in the literature. The results obtained show similarity with the experimental reference data. Complementary, in this study it is also presented a surgical application of the presented computer method, to efficiently create artificial reentry tear configurations and help clinicians in the decision making before the surgical fenestration.

**Segmentation/Program used/Phantom or real:** Ideal model (phantom). Diameter of TL tube is 16mm and the length is 390mm, dissection length of 160mm, proximal and distal tears with diameters between 0 and 10mm, location of the proximal and distal tears from the inlet is 177.5mm and 322.5mm. Different tear size configurations are studied.

**Simulation/Code used/Type of simulation:** KRATOS (open-source simulation code developed by CIMNE). FSI simulation. 3D, meshing using GID.

**Boundary conditions:**

**Inlet:** Parabolic profile (formula) to impose a parabola in the inlet, velocity is time dependent obtained from the experiment [22].

**Outlet:** Pressure waveform directly taken from the experiment measurements in [22].

**Wall (material):** Aortic wall assumed to be rigid.

**Blood density:** 1050 Kg/m<sup>3</sup>.

**Title:** Evaluation and verification of patient-specific modelling of type B aortic dissection.

**Reference:** [23]

**Year:** 2021

**Summary:** This study presents a patient-specific workflow to simulate blood flow in type B aortic dissection, using CT images, 4D-flow MRI, and invasive Doppler-wire pressure measurements. The aim is to evaluate and verify this workflow comparing the CFD simulations with the *in vivo* data. The CFD results showed to be in good agreement with 4D-MRI data, where 80% of the analyzed regions achieved moderate or strong correlations between the predicted and *in vivo* velocities. In addition, the predicted CFD pressures were well matched to the Doppler-wire measurements, with some deviation in peak systolic values.

**Segmentation/Program used/Phantom or real:** Real model (CT and 4D-flow MRI scans). Segmentation performed using Mimics (Materialise HG, Leuven). Computational meshes were generated using ICEM CFD (Ansys Inc, v15.0).

**Simulation/Code used/Type of simulation:** Simulations were run in Ansys CFX (Ansys v20), timestep of 0.001 s. Results were postprocessed using EnSight (Ansys, v20). CFD simulation.

**Boundary conditions:**

**Inlet:** Time-varying-3-dimensional inlet velocity profiles were extracted from the 4D-flow MRI data for each patient.

**Outlet:** Three-element Windkessel model.

**Wall (material):** Aortic wall assumed to be rigid.

**Title:** Role of proximal and distal tear size ratio in hemodynamic change of acute type A aortic dissection.

**Reference:** [24]

**Year:** 2020

**Summary:** The aim of this study is to examine the role of tear size in the hemodynamic change and help improve the treatment level of type A aortic dissection. The study comprised 120 patients distributed in three different groups depending on the proximal and distal tear size ratio (PDTSR). In group A (PDTSR  $\geq 2:1$ ) there were 35 patients, in group B ( $1:2 < \text{PDTSR} < 2:1$ ) 44 patients and in group C (PDTSR  $\leq 1:2$ ) 41 patients. Three different CFD models with different PDTSRs were made for each group. Results showed that patients in group A had a significantly larger proximal tear size, and the mortality was significantly higher than those in group B and group C in the acute phase. Finally, it was found that a proximal tear size larger than a distal tear size was associated with preoperative death.

**Segmentation/Program used/Phantom or real:** Real model (CTA images). Image segmentation and surface reconstruction performed using Mimics 17.0 (Materialise Inc., Belgium). The meshes were generated using HyperMeshv10.0 (Altair Hyperworks, Troy, MI, USA).

**Simulation/Code used/Type of simulation:** Simulations were run with the commercial CFD solver Fluent 15.0 (Ansys Inc., USA). CFD simulation.

**Boundary conditions:**

**Inlet:** Inlet flow waveforms were based on data presented by Mills et al. [25].

**Outlet:** The time-dependent pulsatile flow waveforms at the outlet were obtained from the work of Olufsen et al. [26].

**Wall (material):** Aortic wall assumed to be rigid.

**Blood density:** 1050 Kg/m<sup>3</sup>.

**Viscosity:** 3.5 mPa·s.

**Title:** Prediction for future occurrence of type A aortic dissection using computational fluid dynamics.

**Reference:** [27]

**Year:** 2021

**Summary:** The aim of this study is to elucidate the mechanism of acute type A aortic dissection using CFD analysis. CFD analysis was performed with two models: healthy control model and pre-dissection model, which were generated from computer tomography (CT) images. In healthy controls there was no spotty high oscillatory shear index (OSI) area at the ascending aorta. In pre-dissection patients, systolic WSS was high on the side of the greater curvature of the ascending aorta due to the accelerated aortic flow. On the side of lesser curvature, high OSI areas were observed around the vortex flow and a high spotty OSI area was found close to the actual primary entry site of the future TAAD. In conclusion, the high OSI area with vortex flow is associated with the future primary entry site, so the mechanism of TAAD can be elucidated with CFD analysis.

**Segmentation/Program used/Phantom or real:** Real model (CT images). Image segmentation and geometry reconstruction performed using Osirix (Osirix Foundation, Geneva, Switzerland). Computational meshes were created using the commercial software ANSYS-ICEM CFD 16.2 (ANSYS Japan, Tokyo, Japan).

**Simulation/Code used/Type of simulation:** The solver used to run the simulations was ANSYS-FLUENT 16.2 (ANSYS Japan, Tokyo, Japan). CFD simulation.

**Boundary conditions:**

**Inlet:** Inlet boundaries for the ascending aorta were extruded to 5 times their diameter to develop the velocity profiles, boundary conditions were set as the mass flow boundary conditions with a pulsatile wave.

**Outlet:** Outlet boundaries were extended to 50 times the diameter of each vessel, boundary conditions were set as the pressure boundary conditions.

**Wall (material):** Aortic wall assumed to be rigid.

**Blood density:** 1060 Kg/m<sup>3</sup>.

**Viscosity:** 0.004 Kg/m/s.



**Title:** An integrated fluid-structure interaction and thrombosis model for type B aortic dissection.

**Reference:** [28]

**Year:** 2022

**Summary:** In this study an integrated FSI-thrombosis model has been applied to an ideal type B aortic dissection geometrical model to analyze the interaction between vessel wall motion and growing thrombus. Results show that wall compliance and flap motion can influence the progression of false lumen thrombosis. Increasing the Young's modulus of the flap results in a reduced mobility and it slows down the thrombus growth. Compared to the rigid model, the predicted thrombus growth is 25% larger using the FSI-thrombosis model with a relatively mobile flap. Moreover, the FSI-thrombosis model can capture the gradual effect of thrombus growth on the flow field, leading to flow obstruction in the false lumen, increased blood viscosity and reduced flap motion.

**Segmentation/Program used/Phantom or real:** Ideal model, geometry model obtained from [29].

**Simulation/Code used/Type of simulation:** The solver used to run the simulations was COSMOL Multi-physics v5.2 (COMSOL AB, Sweden). FSI simulation.

**Boundary conditions:**

**Inlet:** Time-dependent flow waveform with a flat velocity profile.

**Outlet:** Three-element Windkessel model.

**Wall (material):** For the aortic wall  $E = 2.7$  MPa and for the intimal flap  $E = 6.75$  MPa. To investigate the effect of thrombosis the intimal flap  $E$  was increased to 60 MPa to simulate a less mobile flap.

**Blood density:** 1060 Kg/m<sup>3</sup>.

**Title:** Coupled morphological-hemodynamic computational analysis of type B aortic dissection: a longitudinal study.

**Reference:** [30]

**Year:** 2018

**Summary:** A longitudinal study was performed for a type B aortic dissection patient, who was diagnosed and treated in 2006 but received surgery in 2010 due to late complications. A geometry model was made for the aorta in 2006 and 2010. The evolution of the FL was quantified with registration algorithms, while with CFD simulations several hemodynamic indexes were computed, including the WSS and the relative residence time. Correlations between hemodynamics and the evolution field in time obtained by registration algorithms is discussed.

**Segmentation/Program used/Phantom or real:** Real model (CTA images). Computational meshes were created using the open-source mesh generator NETGEN (<https://ngsolve.org/>).

**Simulation/Code used/Type of simulation:** The solver used to run the simulations was LifeV. CFD simulation.

**Boundary conditions:**

**Inlet:** Time-dependent flow waveform with a flat velocity profile, the flow rate was adopted from a previous study [31].

**Outlet:** Three-element Windkessel model.

**Wall (material):** Aortic wall assumed to be rigid.

**Title:** Predicting flow in aortic dissection: Comparison of computational model with PC-MRI velocity measurements.

**Reference:** [32]

**Year:** 2014

**Summary:** The aim of this study is to assess the computational models adopted in previous studies analyzing the correlation of the simulation results with the *in vivo* velocity data obtained with phase-contrast magnetic resonance imaging (PC-MRI). CTA images were used to make the geometrical model while PC-MRI velocity data was used to define input boundary conditions. The computational model was able to correctly capture the complex regions of flow reversal and recirculation qualitatively, but quantitative differences are present. Assuming a rigid aortic wall and excluding the arch branches, the model overpredicted the FL flow rate by 25% at peak systole. Nevertheless, an overall good agreement was achieved, validating the computational model for TBAD with a relatively stiff dissection flap.

**Segmentation/Program used/Phantom or real:** Real model (CTA images). Image segmentation and geometry reconstruction was performed using Mimics (Materialise HC, Louvain, Belgium). Computational meshes were created using ANSYS ICEM CFX.

**Simulation/Code used/Type of simulation:** The solver used to run the simulations was ANSYS CFX-Post 12. CFD simulation.

**Boundary conditions:**

Flow boundary conditions were extracted from PC-MRI velocity images. Imaging plane 1 corresponds to the flow rate waveforms in the ascending aorta and imaging plane 2 to the aortic arch.

**Inlet:** Flow waveform derived from imaging plane 2, with a flat through-plane profile.

**Outlet:** Zero relative static pressure was applied across both surfaces.

**Wall (material):** The aortic wall was assumed to be rigid with no-slip.

**Blood density:** 1060 Kg/m<sup>3</sup>.

**Viscosity:** 4 mPa·s.

**Title:** Multi-modality image-based computational analysis of haemodynamics in aortic dissection.

**Reference:** [33]

**Year:** 2016

**Summary:** The aim of this study is to understand the hemodynamics in aortic dissection using medical imaging and CFD. Several models of TBAD were made and the hemodynamics in the dissected aorta was compared to those in an equivalent “healthy aorta” created virtually removing the IF. It was found that there was an increased velocity, pressure, and WSS in the dissection model, as well as alterations in flow distribution, particularly in the narrow TL and around the primary entry tear. The flow patterns were similar to those obtained using 4D PC-MRI. A lumped-parameter heart model was then used to show that there was a 14% increase in left ventricular stroke work when there is dissection. Finally, it was studied the effect of secondary connecting tears and it was found that there were significant changes in the hemodynamics when secondary tears were not included in the model, like increases in flow and drops in peak pressure.

**Segmentation/Program used/Phantom or real:** Real model (CTA and 2D PC-MRI and 4D MRI). Image segmentation performed using the 2D segmentation paradigm introduced by Wang et al. (1999) [34]. Meshes created using boundary layer and local curvature-based refinement.

**Simulation/Code used/Type of simulation:** The solver used to run the simulations was CRIMSON ([www.crimson.software](http://www.crimson.software)). CFD simulation.

**Boundary conditions:**

**Inlet:** Flow waveform derived from the 2D PC-MRI data and mapped to a time-varying parabolic velocity profile.

**Outlet:** Three-element Windkessel lumped-parameter model.

**Wall (material):** Aortic wall assumed to be rigid.

**Blood density:** 1060 Kg/m<sup>3</sup>.

**Viscosity:**  $4 \cdot 10^{-3}$  Pa·s.

## Summary table

The studies presented previously are a taste of what is the current state of the art in FEM simulations to study aortic dissection. In Table 2 are summarized the most important characteristics of each study like the software used and the type of simulations and models performed. This will be very useful to further decide how will the project be carried out.

**Table 2.** State of the art in aortic dissection FEM simulation studies.

<b>Reference</b>	<b>Dissection type</b>	<b>Segmentation program</b>	<b>Numerical code</b>	<b>Simulation</b>	<b>Patient-specific</b>	<b>4D/2D MRI</b>
[15]	Type B	-	KRATOS	FSI	No	-
[16]	Type B	-	Tdyn	CFD	No	-
[17]	Type B	SimVascular	SimVascular	FSI	Yes	4D MRI
[18]	Type A	Mimics	ANSYS	FSI	Yes	-
[1]	Type B	-	KRATOS	CFD	No	-
[23]	Type B	Mimics	ANSYS	CFD	Yes	4D MRI
[24]	Type A	Mimics	ANSYS	CFD	Yes	-
[27]	Type A	Osirix	ANSYS	CFD	Yes	-
[28]	Type B	-	COSMOL Multi- physics	FSI	No	-
[30]	Type B	-	LifeV	CFD	Yes	-
[32]	Type B	Mimics	ANSYS	CFD	Yes	2D MRI
[33]	Type B	-	CRIMSON	CFD	Yes	2D and 4D MRI

### 3. Market analysis

This project is addressed to patients with complicated type B aortic dissection. Aortic dissection affects 3-4 people per 100,000 every year, 40% of the cases being TBAD, with increasing incidence during the past decades. Patients without medical therapy with acute TBAD have an early mortality rate of >50%. Due to severe complications such as rupture or malperfusion, mortality is highest within the first 7 days after TBAD. Data from the International Registry of Aortic Dissection (IRAD) indicated that 25% died within three years after acute TBAD. After discharge, an estimation of 31-66% deaths associated with TBAD occurred, caused by rupture or perioperative mortality from aortic repairs. All these statistics show the importance of aortic dissection and the big market it covers [6, 35].

The median and total yearly costs to treat aortic dissections have increased beyond the rate of inflation. After hospital treatment, a higher percentage of women compared to men use post-hospitalization healthcare services. Hospital readmissions are common after surgery within 1 year of hospital discharge. Reinterventions during a readmission generate the highest median cost with respect to other commonly used post-hospital services [36].

Treatment of aortic dissections requires a considerable capital commitment by the healthcare sector for a disproportionally small percentage of the population. A cost-of-illness analysis study performed in Ontario (Canada) found that the total healthcare utilization costs for the treatment of aortic dissections was \$245.7 million, from which TBADs consumed \$141.8 million of the cost expenditures. The total yearly costs for indexed hospitalizations to treat ADs significantly increased over time, going from \$9 million in 2003 to \$20.7 million in 2016. Regarding the cost of the treatment strategies, open surgery had the highest median cost (\$30,372), followed by TEVAR (\$26,896) and medical therapy (\$11,525). Open surgery and TEVAR resulted in 14.4% and 27.2% rates of readmission, respectively. Reinterventions were costly to the healthcare system, with an overall median cost of \$29,073 (\$24,547 for open surgery and \$34,475 for TEVAR). From the posthospital services, rehabilitation was the one that had a higher median cost, with a value of \$11.9 M [36].

Another study showed that the total cost of the hospital stay was significantly higher among patients undergoing open surgery \$53,371 (\$39,029-\$80,471) than with TEVAR \$45,311 (\$31,479-\$67,960). It was concluded that TEVAR presents an advantage in terms of morbidity, mortality and cost when compared to open surgery in the treatment of TBAD [37].

## 4. Conception engineering

### 4.1- Solutions studied

In this section are presented the different approaches that have been studied to make the project (Table 3). It has been divided in four parts: the software used to make the models, the software used to create the mesh, the software used to run the simulations (solver), and the software used to visualize the results (post-processing).

**Table 3.** Studied solutions for the project.

Studied solutions	
Modelling software	<ul style="list-style-type: none"><li>• AutoCAD</li><li>• Gmsh</li><li>• GiD</li></ul>
Meshing software	<ul style="list-style-type: none"><li>• Gmsh</li><li>• GiD</li><li>• Integrated FEM software</li></ul>
Simulation software (solver)	<ul style="list-style-type: none"><li>• Ansys</li><li>• CRIMSON</li><li>• SimVascular</li><li>• Kratos</li><li>• Elmer</li></ul>
Post-processing software	<ul style="list-style-type: none"><li>• GiD</li><li>• ParaView</li></ul>

#### 4.1.1- Modelling software

**AutoCAD** is a computer-aided design (CAD) software developed by Autodesk that allows you to create precise 2D and 3D drawings. It makes the design process easier, as you can draw objects accurately by setting the exact size and alignment you need, and you can make changes and adjustments easily without having to redraw it every time. To download AutoCAD a license is needed, but it is free for students [38].

**Gmsh** is an open-source 3D element mesh generator with a built-in CAD engine and post-processor. It is built around four modules (geometry, mesh, solver, post-processing), which can be controlled with the graphical user interface (GUI), from the command line, using text files written in Gmsh's own scripting language (.geo files), or through C++, C, Python, Julia, and Fortran application programming interface. Gmsh works better in the modelling and meshing part than in the solver part. Because of this, it has just been considered to do the modelling and meshing [39].

**GiD** is a universal, adaptative, and user-friendly pre and post processor for numerical simulations in science and engineering. It is an open-source software developed by CIMNE, and it is very useful in the design process. GiD is a CAD system that features the widely used NURBS surfaces for the

geometry definition, including several CAD repairing tools and mesh generators. The program works through the GUI, such as AutoCAD, and it is easy to use [40].

#### 4.1.2- Meshing software

To create the mesh several options were considered. One possibility was to use a separate software for meshing than for running the simulation. In that case, the previously mentioned programs of **Gmsh** and **GiD** were considered to do the mesh to further import the mesh file in the solver and run the simulation. Another possibility was to do the meshing in the same program of the solver, as some programs offer this option (integrated FEM software). This could be done using the software of **Ansys**, **CRIMSON**, or **SimVascular**, that are the programs studied that have this option.

#### 4.1.3- Simulation software

**Ansys** is an ecosystem of computed assisted engineering programs for the design, analysis, and simulation of FEA problems. It includes the meshing, solver, and post-processing. Ansys CFX is the software of Ansys dedicated to CFD simulations. It has a modern interface that can be used for a wide range of applications [41]. Ansys has the advantage that everything is integrated in the same software. In addition, it has a very powerful solver and has been used by many researchers in the aortic dissection field. However, it requires a license and, even there is a free license for students, it has some important limitations for CFD simulations.

**CRIMSON** is an advanced simulation environment for subject-specific hemodynamic analysis developed by the University of Michigan and the King's College of London. It is an open-source software that integrates parallel flow solvers, FSI, GUI-based boundary condition specification, data assimilation, medical image processing, mesh generation, translational hemodynamics, and much more [42]. This software has also everything integrated, such as Ansys, so it is more comfortable to use. Moreover, it has been specifically designed for cardiovascular fluid dynamics problems, so it is more focused on the field in which this project is developed. However, it is quite new and few users have used it, so there is scarce information about it.

**SimVascular** is an open-source software developed by Stanford University for image-based cardiovascular modelling and patient-specific simulation, providing a complete pipeline from medical image visualization, segmentation, 3D model construction, and meshing to blood flow simulation and hemodynamic analysis. It has several solvers, for one-dimensional hemodynamic networks, rigid wall simulations, FSI simulations, or zero-dimensional lumped parameter models of vascular networks [43]. This software is similar to CRIMSON, as it is an integrated software designed for cardiovascular applications. In addition, it has more video tutorials, documentation, and example projects. It also has a public forum in which you can post any doubt or problem you have, and any other user or the own creators of SimVascular can help you.



**Kratos** is an open-source software developed by CIMNE for the implementation of FEM to solve engineering problems. It is written in C++ and it is designed to allow collaborative development by large teams of researchers focusing on modularity as well as performance. The software has the capability to perform CSD, CFD and FSI analysis, as well as solving thermal problems [44]. Contrary to the previous programs, Kratos is just a solver, so the pre-processing and post-processing have to be done using another program [11, 45].

**Elmer** is an open-source finite element software for multiphysical problems developed by CSC-IT Centre for Science. It provides a flexible and extensive platform for solving coupled problems involving multiple physical phenomena, such as structural mechanics, heat transfer, electromagnetics, acoustics, and fluid dynamics. It supports both 2D and 3D simulations and offers a wide range of capabilities for modelling complex geometries, material properties and boundary conditions. It has a GUI that allows users to set up the simulation and define the problem parameters and it also provides a command-line interface for advanced users who prefer scripting [46].

#### 4.1.4- Post-processing software

**ParaView** is an open-source software for post-processing visualization and data analysis. It integrates with your existing tools and workflows, allowing you to build visualizations to analyse data quickly. With its open, flexible, and intuitive user interface, you can analyse extremely large datasets interactively in 3D or programmatically using ParaView's batch processing. With this program it is very easy to visualize and analyse the FEM simulation results. Besides, it is widely used in the engineering community, so there are plenty of resources for problem solving [47].

**GiD** is the program that has been mentioned before for the modelling and meshing, but it can also be used for the post-processing. It has two parts: pre-processing and post-processing. The first one is to design the models and generate the mesh, and the second one is to visualize the results. The post-processing in GiD works similar than ParaView, it has many tools for data analysis, and it is easy to use [40].

#### 4.2- Solution proposed

The software that was chosen to carry out the project was different for each part because the needs were different in each case. In the first part a more complex software was needed because a more complex model had to be simulated (3D aortic dissection model). On the contrary, in the second part, the models were simpler (2D), so it was decided to choose a software easier to use. In the following subsections it will be explained more in detail.

#### 4.2.1- Part I

The programs abovementioned were compared and for each section (modelling, meshing, simulation, and post-processing) it was selected the best fit. In Table 3 it is shown the final selection.

**Table 4.** Solutions proposed for the first part of the project.

	Solution proposed	Reference
Modelling software	GiD	[40]
Meshing and simulation software	SimVascular	[43]
Post-processing software	ParaView	[47]

Regarding the software for the modelling, it was concluded that with **Gmsh** it was more complicated to make a design as complex as the aortic dissection. **AutoCAD** and **GiD** offered more tools to make the geometry and the GUI was more complete and easier to use. In **Gmsh** the GUI is simpler, so it is better to design the geometry by coding a script as a .geo file, however this is more complicated, and it was concluded that making the model in a program through a good GUI would be more efficient. Between **AutoCAD** and **GiD** it was thought that **GiD** would be a better option because it is designed to build models for simulations, whereas **AutoCAD** is more general. In addition, **GiD** is the program developed by the research institution in which the project is carried out (CIMNE), so it was more convenient to use it because in case of any problem it would be easier to solve it.

For the meshing and the simulations, it was decided to use **SimVascular**. From the research carried out, it was observed that in most publications the solver used was **Ansys**. However, the free license for students has some important limitations for CFD simulations, so this option was dismissed. Other publications (from CIMNE) used **Kratos** as the solver, but this software is complicated to use and requires more expertise in FEM simulations. As the author was a beginner and just started in this field, it was decided to use a more guided and intuitive software. The best options were **CRIMSON** and **SimVascular**, as both offered a step-by-step pipeline, a GUI easy to use, and several tutorials to familiarize with the software. Moreover, they are specific for cardiovascular applications. Although both programs have similar features, it was decided to use **SimVascular** because it offered more tutorials and example projects, the guidelines were clearer, and it offered a support forum for troubleshooting. **SimVascular** integrates TetGen software for mesh generation, so it was decided to do the mesh with **SimVascular** as well. The model will be imported in the “Models” section of the **SimVascular** pipeline as a STL file which is exported from **GiD**, and then the pipeline will be followed going through the meshing and simulation.

Finally, the **ParaView** software will be used for the post-processing. It has been chosen to use **ParaView** instead of **GiD** because it is more widely used, so there are plenty of tutorials in YouTube that can be very useful. In addition, the author was feeling more comfortable with this program because had previous knowledge about it.

#### 4.2.2- Part II

In Table 5 are shown the solutions selected for the second part of the project. Due to the problems experienced with **SimVascular** in the first part, for the second part it was decided to simplify the models and use another program. As the aim was to create 2D axisymmetric models, it was decided to use **Gmsh** as the modelling and meshing software because this type of models can be easily coded in a .geo file in **Gmsh** and as they are parameterized, they can be easily modified if needed. The meshing was also performed using **Gmsh** because it was more convenient to do it in the same program and because **Gmsh** is specialized in mesh generation, so it was thought that the result would be better.

Regarding the solver, it was chosen to use **Elmer** because it is open source, it offers the possibility to perform axisymmetric FSI simulations with 2D models and the author felt more comfortable using it. Contrary to **SimVascular**, this program allows the simulation of 2D models and different domains can be easily defined, whereas in **SimVascular** is more complicated. Therefore, by using **Elmer**, the process was simplified.

Finally, the the **ParaView** software was chosen for the post-processing, for the same reasons mentioned in the first part.

*Table 5. Solutions proposed for the second part of the project.*

	Solution proposed	Reference
Modelling and meshing software	Gmsh	[39]
Simulation software	Elmer	[46]
Post-processing software	ParaView	[47]

## 5. Detail engineering

### 5.1- Part I

#### 5.1.1- Healthy aorta

##### *Modelling and meshing*

To design the model of the healthy aorta and the aortic dissection, the software GiD was used. Before starting to make the model, the dimensions of the aorta were determined. It was found that the aorta has a length of 30 cm [48] and that the diameter slightly varies depending on the section of the aorta. As the objective was to study a type B dissection, that is produced in the descending aorta, the corresponding diameter was used, which is 2.5 cm [48]. Therefore, the healthy aorta was modelled as a cylinder with a diameter of 2.5 cm and a length of 30 cm (Figure 3).

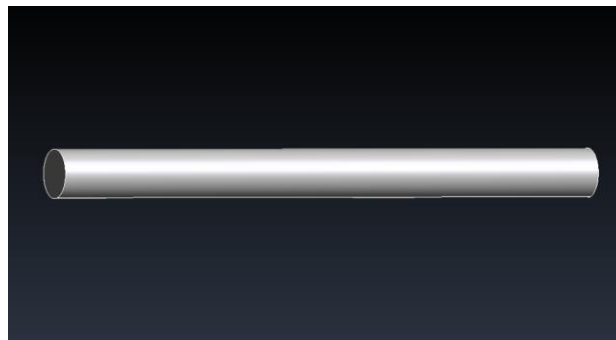


**Figure 3.** Healthy aorta model [own source].

To import the model into SimVascular the GiD file was exported as a STL file. STL files describe only the surface geometry of a 3D object, so the volume of the cylinder had to be eliminated and the surface had to be meshed to further export it as a STL file. Different mesh sizes were tried because it was noticed that the size of the elements of the mesh generated by GiD affected how the model looked like when it was imported in SimVascular. An example is shown in Figure 4 and Figure 5. With an element size of 0.5 (Figure 4), the section of the model when it was imported into SimVascular wasn't completely circular, whereas when reducing the element size to 0.1 (Figure 5), this problem was solved.

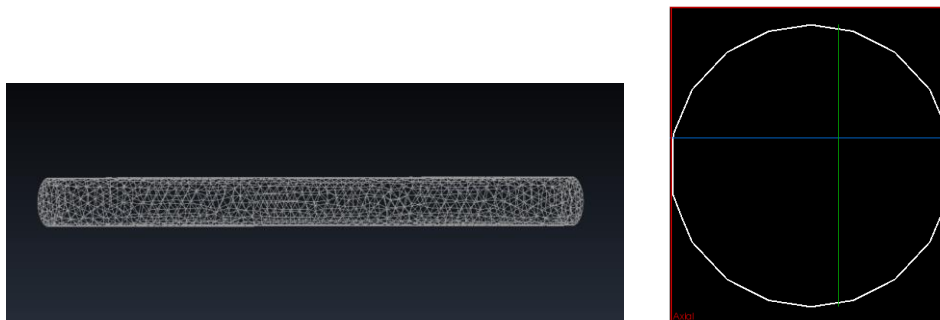


**Figure 4.** Healthy aorta STL model with mesh element size of 0.5 [own source].



**Figure 5.** Healthy aorta STL model with mesh element size of 0.1 [own source].

When the model is imported into SimVascular the faces of the model are automatically detected by the program, but the type of the faces (if they are wall or cap) has to be manually selected, as well as changing the names of the faces. This can be observed in Figure 6, where the faces of the aortic wall, the inlet and the outlet are defined.

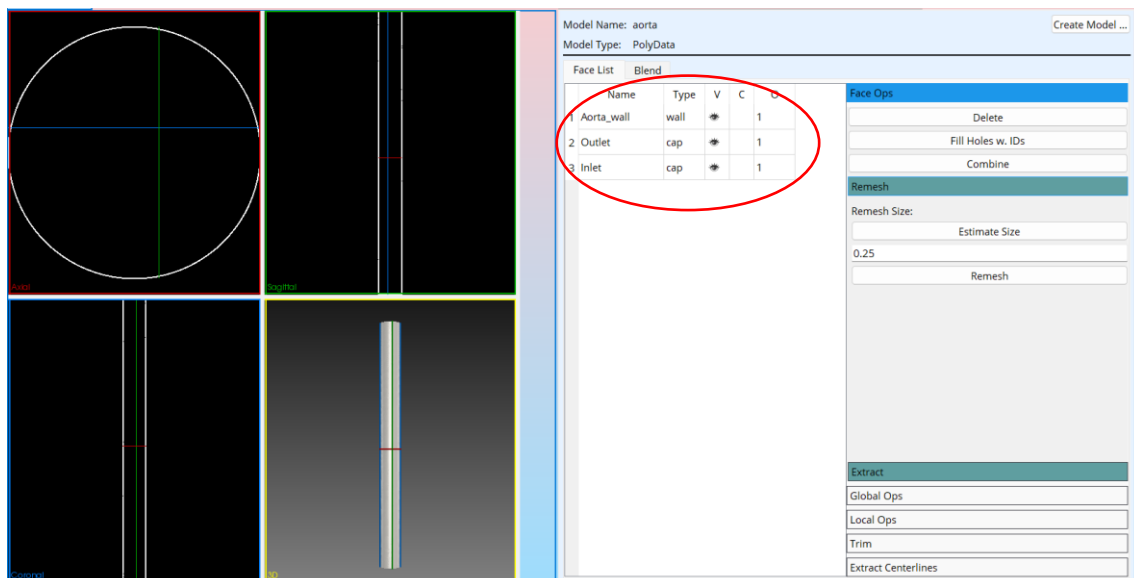


**Figure 6.** Model section of the pipeline in SimVascular [own source].

Once the model is imported, a second meshing has to be performed in SimVascular because is a mandatory step before the simulation (the meshing performed in GiD is just to obtain the STL file). There are several options for the meshing, but the predetermined options were used. SimVascular has a tool that estimates the appropriate element size for the mesh according to the model, and this estimation size was used (Figure 7).

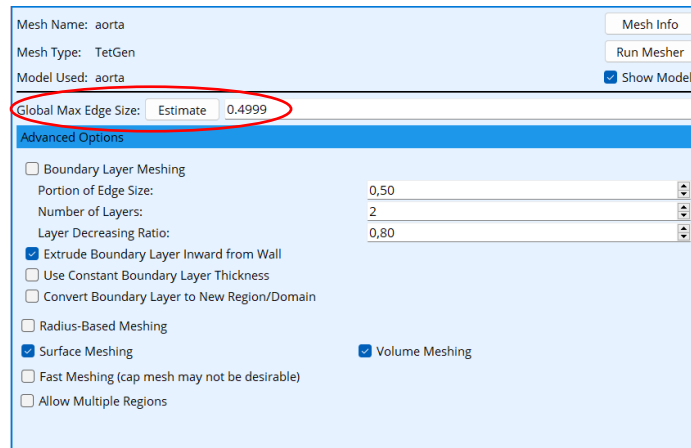


**Figure 7.** Mesh section of the pipeline in SimVascular [own source].

### Simulation

For this model 3 different types of steady state simulations were run:

1. Rigid wall and output resistance
2. Rigid wall and output RCR
3. Deformable wall with uniform wall properties and output RCR

The basic parameters were the same for all the simulations, which are the ones predetermined in SimVascular, and they are shown in Table 6.

**Table 6.** SimVascular basic parameters.

Parameter	Value
Blood density	1060 Kg/m <sup>3</sup>
Blood viscosity	0.004 Pa·s
Initial pressure	0 Pa
Initial velocities	(0.0001, 0.0001, 0.0001) cm/s

Regarding the boundary conditions, the one at the inlet was also the same for the 3 simulations whereas the output boundary condition was different between the first one and the other ones. In the inlet, an inflow waveform file was provided with the format shown in Table 7. The values of the flow are negative because SimVascular considers the positive direction as the normal (vector pointing out of the model), so the flow will need to be negative to represent it going towards the volume.

**Table 7.** Flow imposed at the inlet in SimVascular.

Time (s)	Flow (cm <sup>3</sup> /s)
0	-100.0
1	-100.0

The outlet boundary condition was set as a single resistance of 1333 dynes·s/cm<sup>5</sup> (units in which SimVascular works) for the first simulation. This resistance will give a (weakly-applied) pressure at the outlet face of:

$$p = p_0 + RQ = 0.0 + 1333.0 \cdot 100.0 = 133300.00 \text{ dyn/cm}^2 \approx 100 \text{ mmHg}$$

For the other simulations, the RCR lumped parameters condition was defined as the outlet boundary condition (three-element Windkessel model), in which the behaviour of the downstream vasculature is represented by three parameters: a proximal resistance,  $R_p$ , a capacitance  $C$ , and a distal resistance  $R_d$  (Table 8).

**Table 8.** RCR values employed in SimVascular in CGS units.

RCR parameter	Value
$R_p$	121
$C$	0.000015
$R_d$	1212

The other difference between the simulations was the type of wall. In the first two simulations the wall was set to be rigid, whereas in the third one it was set to be deformable (constant), which means that the wall is deformable with uniform properties (Figure 8). In this configuration different properties have to be set such as the thickness, the elastic modulus (Young's modulus), the density and the pressure. The Poisson ratio and the shear constant are already predetermined and, although they can be changed if wanted, in this case it was left the predetermined value. The thickness was set to 1.6 mm, because it is the thickness of the aortic wall in the descending aorta [49]. The Young's modulus of the aorta was found to be 3 MPa [50], and the density 1050 Kg/ m<sup>3</sup> [51]. The value of the pressure used was the one recommended by SimVascular for cylindrical models, which is estimated from the simulation result of the RCR rigid simulation.

Wall Properties	
Type:	Deformable(Constant)
Thickness:	0.16
Elastic Modulus:	30000000
Poisson Ratio:	0.5
Shear Constant:	0.833333
Density:	1.05
Pressure:	133300

**Figure 8.** Properties of the aortic wall in the deformable model in CGS units [own source].

The last step before running the simulation is to set the solver parameters. There are many parameters but only few of them are required. The ones that were defined are shown in Table 9.

**Table 9.** Solver parameters introduced in SimVascular.

Solver parameter	Value
Number of Timesteps	500
Time Step Size	0.001
Number of Timesteps between Restarts	20

## Post-processing

As previously mentioned, the post-processing of the results was performed with ParaView. The first post-processing step was to use the calculator to transform the pressure units from dynes/cm<sup>2</sup> (the units that gives SimVascular) to mmHg. Then, the tool “Plot Over Line” was used to plot the pressure distribution, in which a line was drawn from the inlet to the outlet crossing the aorta through the centre (Figure 9). Once it was applied, the pressure distribution graph could be observed, as it will be further showed in the results section. The same tool was also used to analyze the velocity at the inlet.

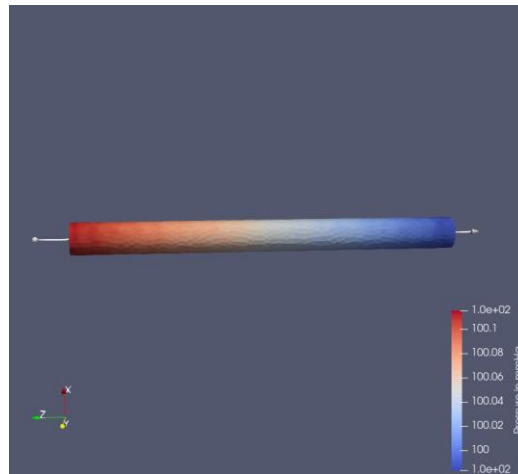


**Figure 9.** Plot over line process in the results of the first simulation [own source].

### 5.1.2- Aortic dissection

The aortic dissection was modelled making the intersection of several cylinders. The first cylinder represents the TL, whereas the second cylinder represents the FL (dissection). To make the model, it was taken the geometry used in the study of Pavel et al. [15]. The dimensions are as follows: TL diameter D1=14mm, FL diameter D2=40mm, FL length L1=160mm, TL length L2=390mm.

To make the model, first two cylinders were created: one for the TL and another one for the FL, intersecting with each other in the Z direction. The corresponding diameter was set for each one of them, but both were created with the same length (the one of the FL). Then, the intersection between both was removed, leaving the TL at the bottom and the FL on the top. To make the entry tear, another cylinder was made perpendicular to the TL and the FL (in the X direction). It was performed the intersection between the surface of this cylinder and the surface of the face between the TL and FL (intimal flap). The result of this process was a circular surface on the intimal flap, representing the entry tear. Finally, the extremes of the TL were extruded to obtain the correct length of the TL (L2). The final model can be observed in Figure 10, where the TL is in grey, and the FL is in blue. The entry tear can be observed as a small circle between both.



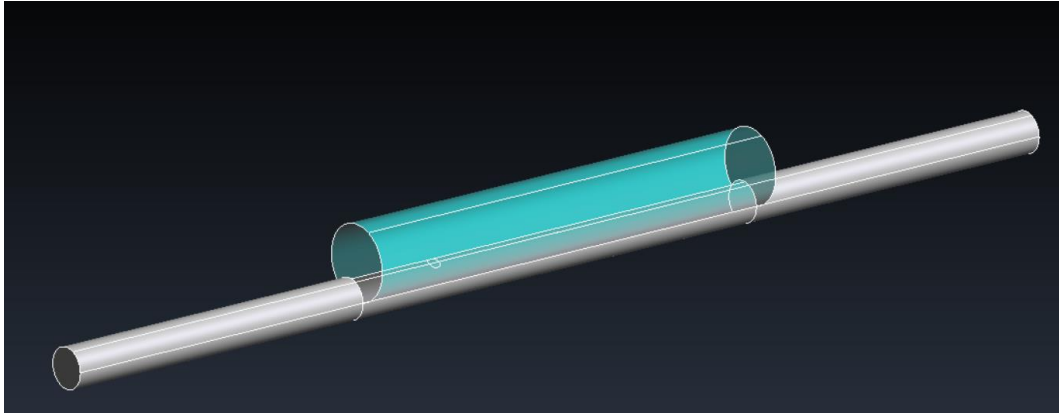


**Figure 10.** Aortic dissection model [own source].

In this case, the mesh was directly generated using an element size of 0.1, as it worked well with the healthy aorta model, and it was also exported as STL. However, when the model was imported into SimVascular, there was an issue. It was observed that the faces of the model were not correctly detected by SimVascular (Figure 11). Instead of identifying the TL and FL as separate entities, they were detected as a single one. Several tests were conducted to solve this problem, but they didn't result, so the simulations couldn't be carried out and this part of the project had to be abandoned.

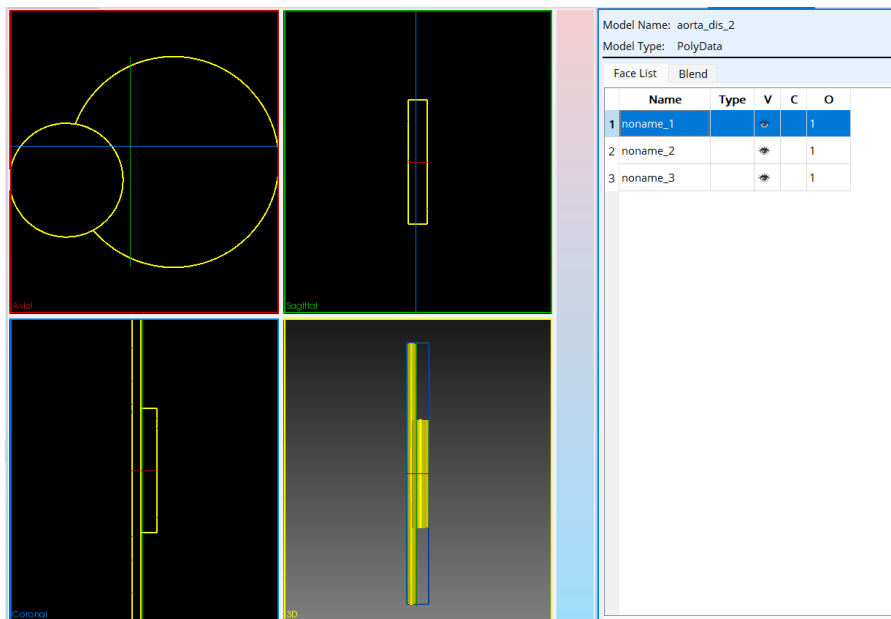


**Figure 11.** Model faces identification in SimVascular [own source].

## 5.2- Part II

### 5.2.1- Modelling

The first step is to design the model of the three cases: the healthy aorta, the dissected aorta with the stent graft and the dissected aorta with the patch. In order to simplify the modelling process and the simulation, a 2D model was designed. The dimensions of the model were the same as the ones used for the healthy aorta model in the first part:  $D = 2.5 \text{ cm}$ ,  $L = 30 \text{ cm}$ ,  $t = 1.6 \text{ mm}$ .

Once the dimensions were known it was started the design process. The aortic lumen and wall were modelled as two adjacent rectangles with the abovementioned dimensions. This was common in the three models; however, the difference was in the aortic wall. For the stent graft and the patch models, the aortic wall was divided into different sections corresponding to different materials whereas for the healthy aorta there was a single section. In Figure 12 it can be observed how the designed looked like.

In the stent graft model, the aortic wall was divided into three sections. The middle section corresponds to the stent graft along the aortic dissection whereas the other two sections correspond to the healthy aortic wall.

In the patch model, the aortic wall was divided into four sections. Like in the stent graft model, the first and last sections correspond to the healthy aortic wall. But in this case instead of a single middle section there are two, one corresponding to the patch (after the first section of healthy aorta) and the other corresponding to the aortic dissection. The section corresponding to the patch was made shorter because the patch is made to just cover the entry tear of the aortic dissection, and not the whole aortic dissection as the stent graft.

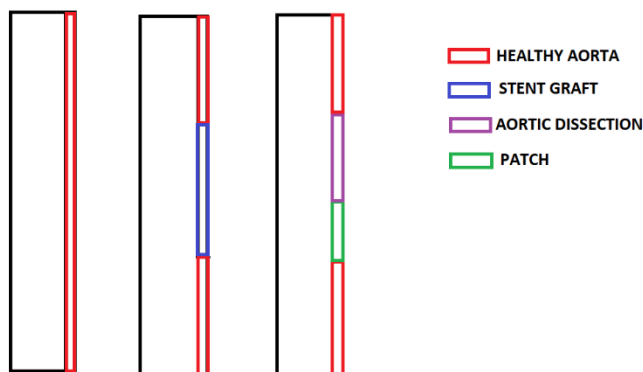


**Figure 12.** Sketches of the models to be designed [own source].

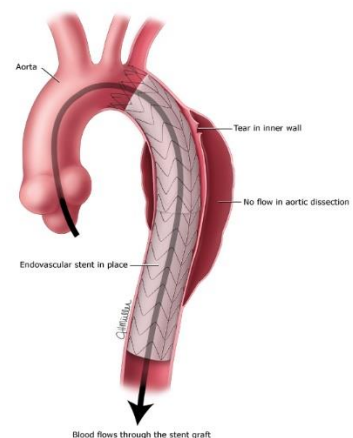


**Figure 13.** Endovascular stent graft for aortic dissection. Extracted from [52].

In the stent graft model, there wasn't an aortic dissection part because the stent graft is placed along all the aortic dissection, forcing the blood to flow through the stent (Figure 13). Therefore, the properties of this section are actually the properties of the stent. On the contrary, in the patch model,

the patch has a small size and just covers the entry tear to avoid the blood inflow, so just a small part of the wall will have the properties of the patch whereas the rest will have the properties of the aortic dissection. As the dimensions of the patch were not known, an approximated model was created.

To make the models the Gmsh software was used. Instead of using the GUI, the model was made by writing a .geo file with Notepad++ (a free source code editor) using Gmsh programming language. This was done to have a better control over the different parameters of the model. First, the parameters of the length, radius, and thickness were defined, as well as the element size. Then the first point was defined (point at the origin of coordinates). This point was extruded twice in the X direction to generate the other two points of the bottom lines, the line for the fluid and the line for the wall. These two lines were then extruded in the Y direction to generate the other lines, and in this process the surfaces of the fluid and the wall were defined, as well as some important lines that we will further need, like the interface line between the fluid and the wall. Finally, this file was imported in Gmsh, and the model could be visualized in the GUI, as well as all the physical entities defined.

### 5.2.2- Meshing

The mesh generation consists of the subdivision of a continuous geometric space into discrete geometrical and topological cells, like rectangles or triangles. The mesh size is very important in FEM because very big elements give bad results, but very small elements make computing too long, so you don't end up getting results at all. The optimal is to find the balance between both extremes.

The size of the mesh can be modified in the .geo file where the model is created. As mentioned before, one of the parameters defined is the element size that defines the size of the elements in the mesh. However, the number of elements in the mesh is controlled by the layers that are set in the extrusion. In this case, it was thought that the optimal would be to have in the X direction 10 elements in the fluid domain and 3 elements in the wall domain (Figure 14). Therefore, the layers of the extrusion of the first point were set to 10 and the layers of the extrusion of the second point were set to 3.

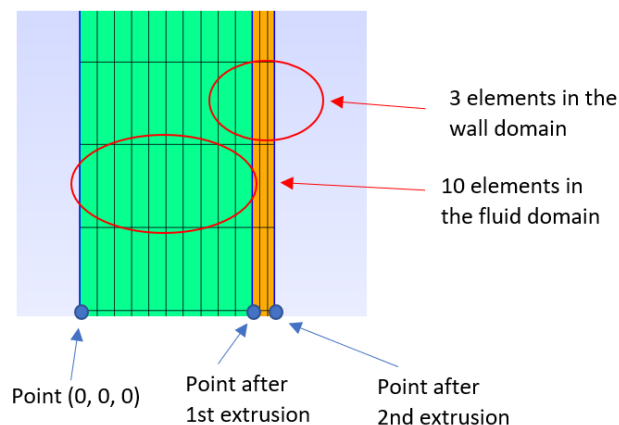


**Figure 14.** Mesh generation in GMSH [own source].

In the Y direction it was decided to define 50 elements along the Y direction. In the case of the healthy wall model this would mean to set the number of layers to 50 because there is only one extrusion. However, in the stent graft model and the patch model, as the aortic wall is divided in sections, there are as many extrusions as number of sections, so the layers per extrusion were adjusted accordingly.

In Figure 15 is shown how would the models with the mesh look like but the length of the models in the figure has been reduced to 10 cm to be able to correctly visualize the different wall sections (because with 30 cm it was so long that it was not possible to make a zoom in which all the sections can be visualized).

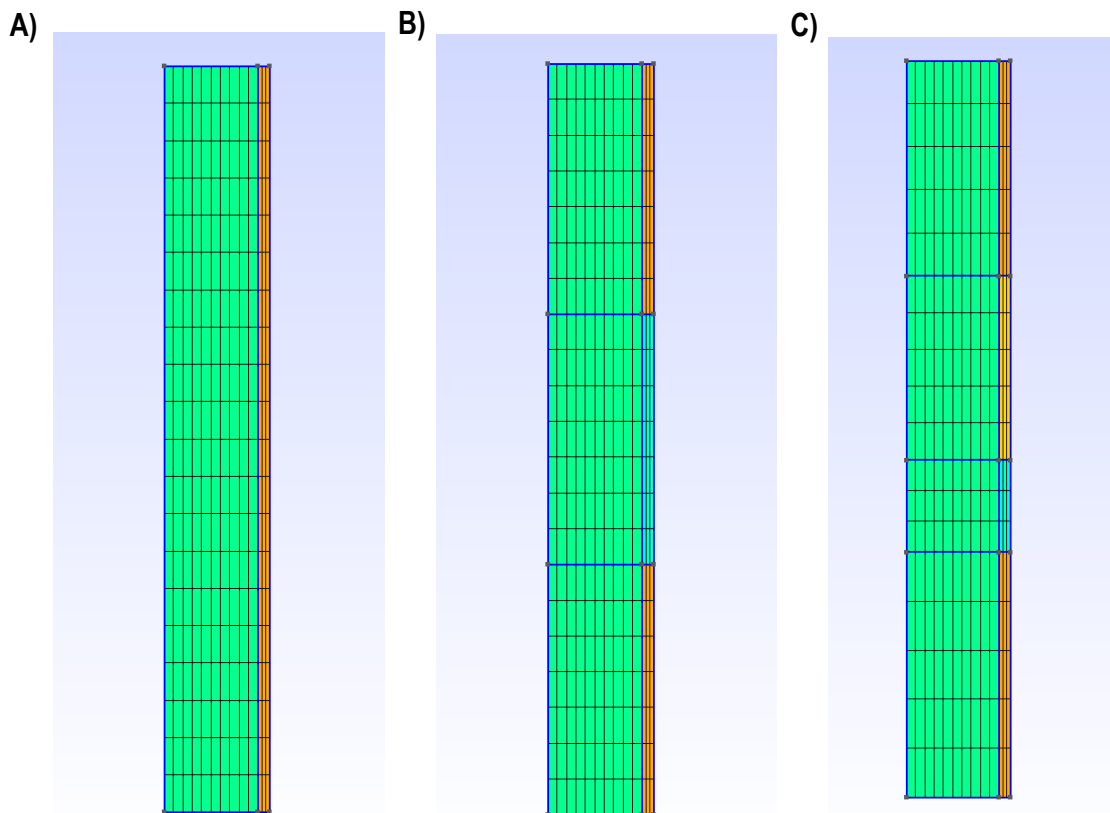


**Figure 15.** Meshed model of the healthy aorta (A), aorta with stent graft (B), and aorta with patch (C) [own source].

### 5.2.3- Simulation

The FEM simulations were performed with Elmer, which offers the possibility to make fluidic FSI simulations. To make the simulations there is a pipeline that has to be followed. First, we need to import the mesh that we have created with GMSH and complete the simulation set up, in which you set the name of the .sif file and .vtu files that will be generated, the coordinate system, the type of simulation, the steady state maximum iterations, and the timestep intervals and sizes (among other parameters). Then the governing equations are imposed for the fluid domain and the solid domain. The next step is to set the material properties, in this case the blood and the aortic wall. After that, the initial conditions are imposed and finally the boundary conditions, which are constraints necessary for the solution of the equations.

## Set up

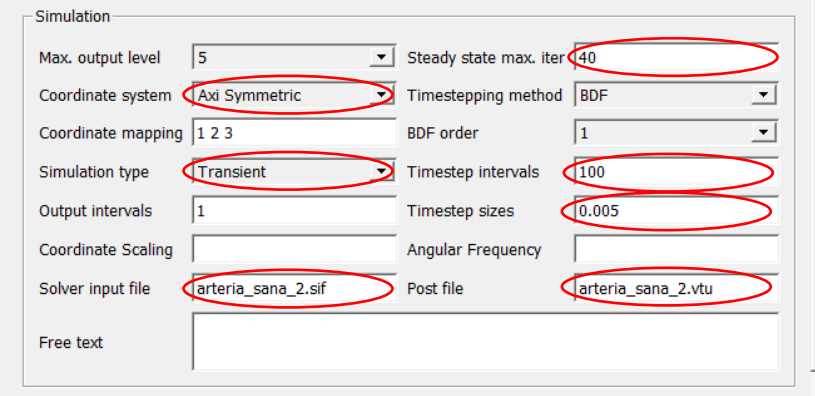
The same set up was used for the simulations in all the models. The parameters that were modified from the predetermined are the ones highlighted in Figure 16.

First of all, it was implemented an axisymmetric simulation. Axisymmetric simulations are numerical techniques used to analyze structures that exhibit rotational symmetry around an axis. The problem and the geometry are simplified by assuming that the geometry and loading conditions are symmetric about the central axis. This way a 2D model can be simulated in 3D, without having to make a 3D model, that would be more complex.

Moreover, it was decided that transient simulations would be performed because the objective is to compare the pressure waveforms of the different models and to obtain the pressure waveform it is necessary to obtain the pressure as a function of time, therefore the equations have to be solved for different time intervals. This leads to the parameters of “Timestep intervals” and “Timestep sizes”, which are related to transient simulations. To clearly capture the pressure waveform, it is required a small timestep because it propagates fast and with a large timestep the proper shape of the wave wouldn't be captured. After several trials, the smallest timestep size that could be used for the solution to converge was 0.005, and a number of 100 timestep intervals was sufficient to observe the wave.

Another important parameter is the number of steady state max iterations, which is the maximum number of iterations for obtaining convergence for every steady state or time point. It should be big for nonlinear problems, like the one we want to solve, so the value was set to 40.

Finally, the name of the solver input file and the post file was written, so that the name represented that particular simulation. In Figure 16 is shown the one relative to the healthy aorta simulation.



The screenshot shows a 'Simulation' configuration window with the following parameters and values:

Parameter	Value
Max. output level	5
Steady state max. iter	40
Coordinate system	Axi Symmetric
Timestepping method	BDF
Coordinate mapping	1 2 3
BDF order	1
Simulation type	Transient
Timestep intervals	100
Output intervals	1
Timestep sizes	0.005
Coordinate Scaling	
Angular Frequency	
Solver input file	arteria_sana_2.sif
Post file	arteria_sana_2.vtu
Free text	

**Figure 16.** Set up of the simulation [own source].

## Equations

The equations are what the solver will compute to obtain the results, so it is important to determine which are the equations that better define the behaviour of the model. In this case, there are two domains in the models: the fluid domain and the solid domain. The fluid domain corresponds to the blood and it is described by the Navier-Stokes equation, as it is considered an incompressible fluid.

The solid domain corresponds to the aortic wall, and it is described by the non-linear elasticity equation, because the aortic wall has a non-linear behaviour. Besides these two equations, it is necessary to add the equation of the mesh update in the fluid domain because the fluid will be deformed in every iteration, and the mesh will need to be updated every time to start from the correct geometry in the next iteration. In Figure 17 and Figure 18 is shown how to set these equations into Elmer. For each case it is just necessary to activate the equation and assign it to the corresponding body (blood or wall). In addition, a priority needs to be assigned, being the higher number the one with more priority. The Navier-Stokes has the highest priority (Priority = 3), followed by the nonlinear elasticity (Priority = 2) and lastly the mesh update (Priority = 1). This just indicates the order in which the equations are solved.

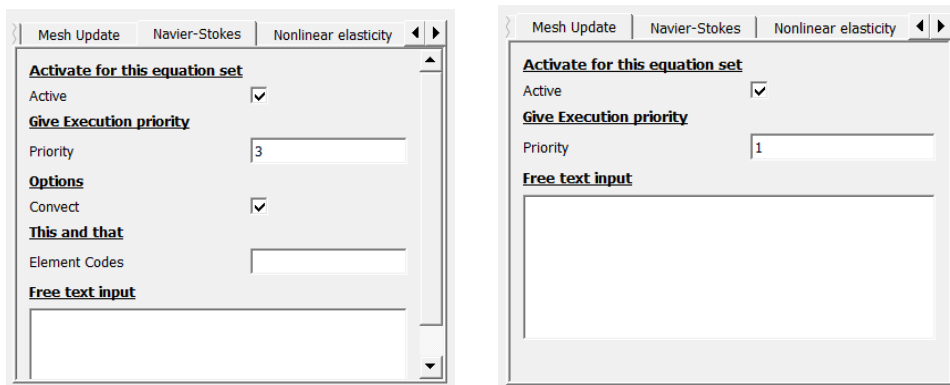


**Figure 17.** Blood equations (Navier-Stokes and Mesh Update) [own source].

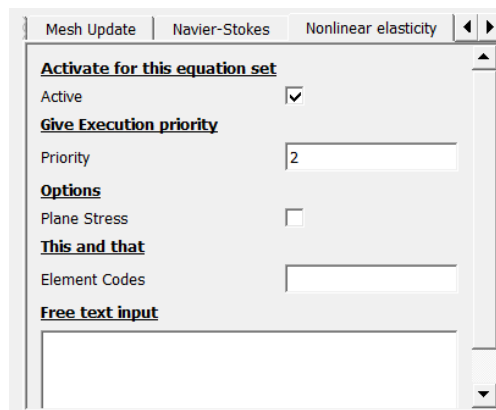


**Figure 18.** Aortic wall equation (Nonlinear elasticity) [own source].

Elmer has also the option to modify the solver settings. For the Navier-Stokes solver and the nonlinear elasticity solver some parameters had to be modified for the solution to converge. For the Navier-Stokes, the method chosen was BiCGStabl (iterative method) with order 4 and the preconditioning chosen was BILU0 (Figure 19). For the nonlinear elasticity the method chosen was Umfpack (direct method), that is the one needed for nonlinear problems (Figure 20).

**Figure 19.** Solver Settings of the Navier-Stokes [own source].

**Figure 20.** Solver settings of the non-linear elasticity [own source].

## Materials

The blood properties to be defined are the density and the viscosity. It was found that in other studies they set the density to 1060 Kg/m<sup>3</sup> and the viscosity to 0.004 Pa·s, so the same values were used in the simulations of this project [27, 12]. Moreover, for the mesh update it was set the Young's modulus to 1 Pa and the Poisson ratio to 0.3.

The properties to be defined for the aortic wall are the density, the Young's modulus and the Poisson ratio. However, as previously mentioned, the material properties of the aortic wall were different depending on the model and the wall section. In Table 10 are shown all of them.

**Table 10.** Material properties.

	Density	Young's modulus	Poisson ratio
Healthy aortic wall	1050 Kg/m <sup>3</sup>	3 MPa	0.45
Stent graft	7860 Kg/m <sup>3</sup>	210 GPa	0.45
Aortic dissection wall	2000 Kg/m <sup>3</sup>	1.3 MPa	0.45
Patch	1050 Kg/m <sup>3</sup>	2.7 MPa	0.45

The wall was considered to be incompressible, as well as the stent, so that's why the Poisson ratio is 0.45 in all the cases. A completely incompressible material would have a Poisson ratio of 0.5, but it was set to 0.45 because putting the maximum can sometimes generate troubles in the simulation.

Regarding the other properties, it was found that the healthy aorta has a Young's modulus of 3MPa [50] and a density of 1050 Kg/ m<sup>3</sup> [51]. The stent graft was defined to be of stainless steel because it is the most common, and it has a Young's modulus of 210 GPa [53] and a density between 7500 Kg/m<sup>3</sup> and 8000 Kg/m<sup>3</sup> [54], so a density of 7860 Kg/m<sup>3</sup> was chosen because is a value in the middle of this range. The aortic dissection was found to have a Young's modulus of 1.3 MPa [55] and a density of 2000 Kg/m<sup>3</sup> [15]. Finally, the properties of the patch were not known but it was known that it was similar to the healthy aortic wall, so it was decided to set the Young's modulus to 10% less than the one of the healthy aorta, obtaining a value of 2.7 MPa, and the same density as the healthy aorta (1050 Kg/m<sup>3</sup>).

### *Initial conditions*

Just one initial condition was imposed in the model, which is an initial pressure of 10,000 Pa (Figure 21). This condition means that at t = 0 the pressure will be 10,000 Pa in the whole domain. This way all the points have an initial pressure and there isn't such an abrupt change in the pressure when the fluid flows through the inlet.

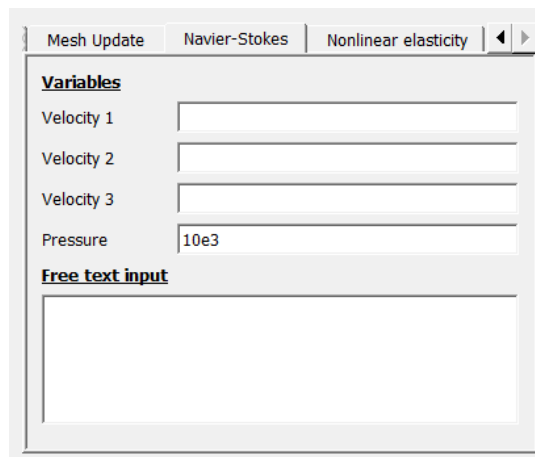


**Figure 21.** Initial conditions [own source].

### *Boundary conditions*

In all the models 5 boundary conditions were imposed:

1. **Axisymmetry:** in the central axis it was imposed the mesh update and velocity in the X and Y direction to be 0, so that the points are not moved, and the symmetry is maintained (Figure 22).



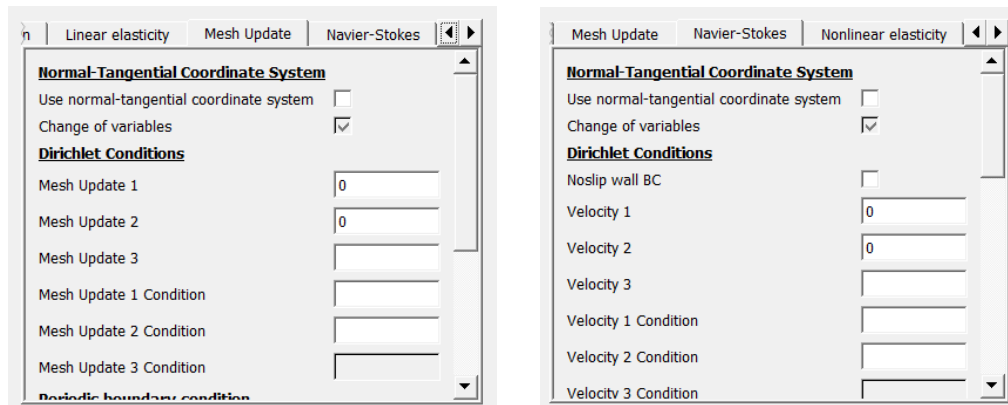


Figure 22. Axisymmetry boundary condition [own source].

- FSI:** it is the interaction of a moveable or deformable solid structure with an internal or surrounding fluid. In this case, by imposing this condition the interaction between the blood and the deformable aortic wall is taken into account, which is essential for simulating the blood flow. To impose this condition in Elmer it just has to be activated and assigned to the line that separates the blood and the wall (Figure 23A). In addition, it was imposed that the mesh update in the X and Y direction is the same as the displacement in these directions to update the mesh as the fluid deforms the wall (Figure 23B). Finally, it was also imposed that the velocity in the X and Y direction in this interface is the same as the mesh velocity in these directions (Figure 23C).

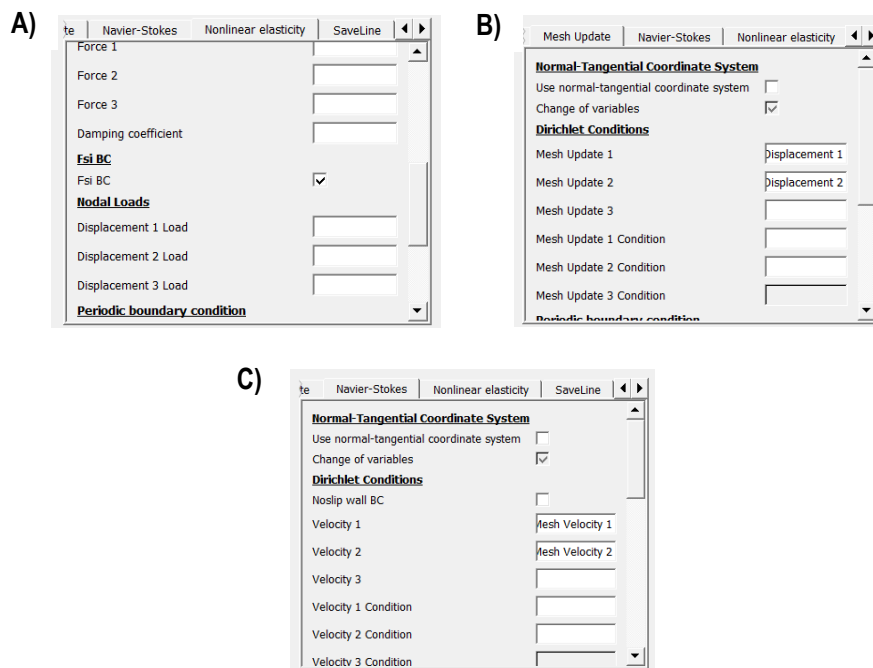


Figure 23. FSI boundary condition [own source].

- Clamp:** this boundary condition consists of fixing the ends of the vessel to avoid a chaotic movement when it deforms. To achieve it, the displacement of the wall in the X and Y direction was set to 0, blocking the movement in any direction (Figure 24).

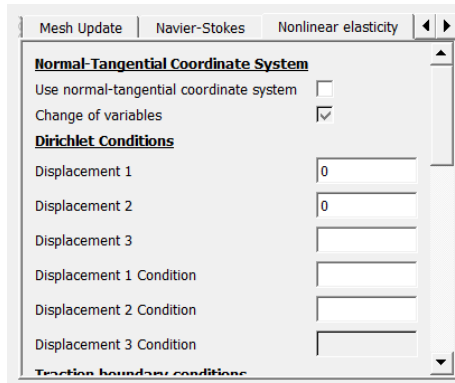


Figure 24. Clamp boundary condition [own source].

4. **Outlet pressure:** in the outlet it was set a constant pressure of 10,000 Pa because it is the pressure that was set at time 0 at the outlet in other studies of aortic dissection FEM simulations [1, 15]. In the other studies it was applied a pressure waveform, in which the pressure of 10,000 Pa was just the first value and this one changed with time (Figure 25). However, in this case a constant pressure was applied to simplify the simulation (Figure 26). It can be observed that the external pressure applied is negative. This is because Elmer takes the positive direction as the normal (vector pointing out of the surface), so as it has to be applied towards the vessel, it has to be negative.

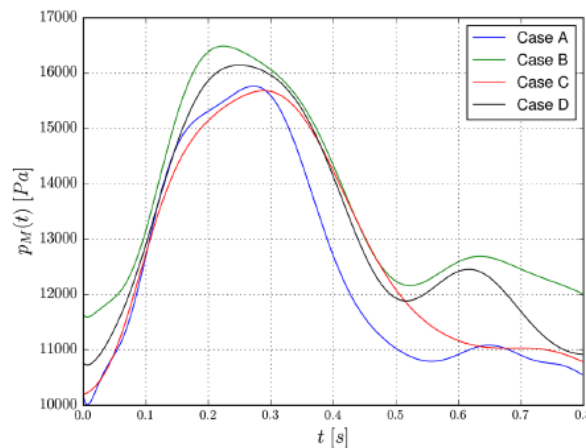


Figure 25. Pressure at the outlet in the study of Zorrilla et al. Extracted from [1].

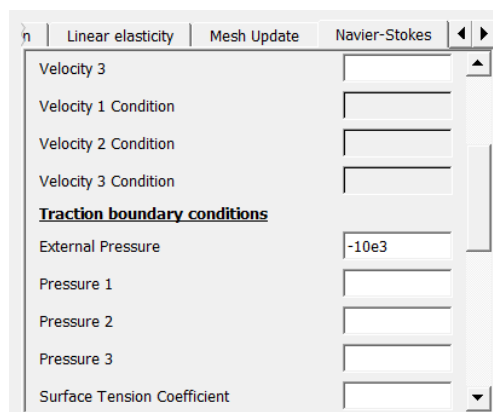
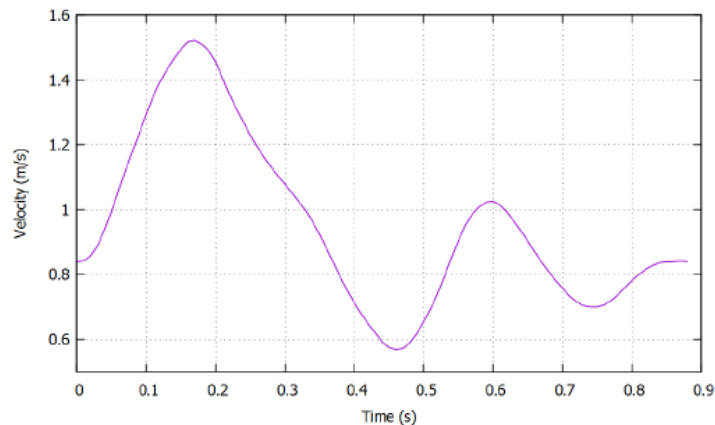


Figure 26. Pressure at the outlet in Elmer [own source].

5. **Inlet velocity:** at the inlet it was applied a velocity waveform so that the velocity changed with time. This waveform was defined by the following equation (Eq.1):

$$v = \left( 1 - \left( \frac{x^2}{r^2} \right) \right) \cdot 2\sin(2\pi t) \quad (1)$$

Where  $v$  is the velocity,  $x$  is the space coordinate in the X axis,  $r$  is the radius of the aorta,  $2\pi$  is the angular velocity, corresponding to a frequency of 1 Hz, and  $t$  is the time. The first part of the equation is to give the velocity a parabolic profile, so that the velocity is maximum in the centre and is minimum next to the wall. The second part of the equation (sine function) corresponds to the waveform that causes the velocity to change with time. The sine function is multiplied by 2 to give velocity values in the correct range. The reference range was taken from another study, in which they also apply a velocity waveform at the input and have values approximately between 0.8 m/s and 1.5 m/s (Figure 27), in which the maximum is the normal systolic velocity, with a value of 1.5 m/s. In the simulations performed, the velocity range was similar but slightly larger, taking values between 0 m/s and 2 m/s (Figure 28). In Figure 28 is shown the velocity waveform for one pulse, which has a period of 1s in total, so the wave has a duration of 0.5s and the flat part (velocity = 0) has a duration of 0.5s. By making the pulse of 1s and the frequency of 1Hz, a cardiac frequency of 60 bpm is established.



**Figure 27.** Velocity at the inlet in the study of Pavel et al. Extracted from [15].

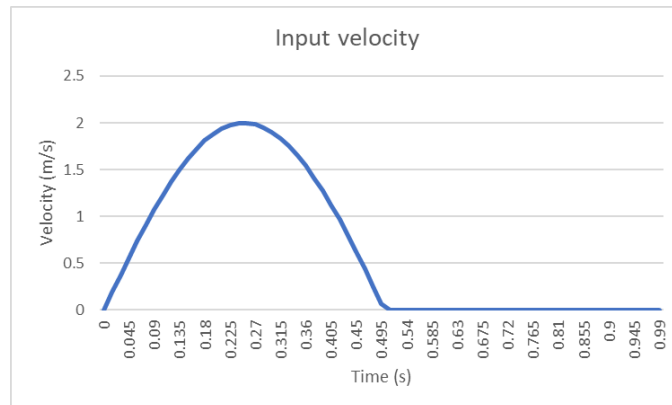


**Figure 28.** Velocity imposed at the inlet in Elmer [own source].

#### 5.2.4- Post-processing

As the simulations performed are transient simulations, the results obtained are for every time interval. The objective is to obtain the pressure waveform and determine how the pressure changes with time. This was performed studying the time evolution of the pressure at one point of the model, which has to be the same in the three models. To correctly compare the results of the models, a point in the inlet was selected to avoid the distortion of the generated pulse by the different materials. The tool of “Find data” was used and the coordinates  $X = 0$ ,  $Y = 0$ , and  $Z = 0$  were introduced to select the first point at the centre of the inlet. Finally, the tool “Plot Selection Over Time” was used to obtain the pressure waveform of this point.

### 5.3- Results and discussion

#### 5.3.1- Part I

As previously mentioned, for this first part just the results from the healthy aorta model could be obtained. Three different simulations were performed and in this section the results will be presented and discussed.

To determine the differences between the simulations, the pressure distribution was assessed. In the following figures it can be observed the visual and graphical representation of the pressure distribution for each simulation. In the first case (Figure 29), the pressure follows a clear linear distribution, where the maximum pressure is at the input ( $x = 0$  cm) and the minimum is at the output ( $x = 30$  cm). In the second case (Figure 30) it can also be observed that the pressure decays linearly but there is more variation than in the first case. It can be observed also in the visual representation, where the colouring shows that the pressure is not uniformly distributed. This could be because of the RCR at the outlet that, contrary to the first case, adds a capacitor that represents the blood stored in peripheral vessels, so it considers the elasticity of the arteries [56]. This blood that is progressively stored and released acts as a resistance variable in time, which alters the flow through the vessels, and consequently the pressure. Finally, in the last case (Figure 31), that is the simulation with the deformable wall, it can be observed that the pressure distribution is not linear, but instead it is slightly curved. As the wall is deformable the diameter of the aorta changes, and if the diameter changes the resistance also changes, causing a non-linear distribution.

Looking at the pressure values, it can be observed that both rigid models are within the same range of pressures, being the maximum of 100.11 mmHg or 100.13 mmHg (for the first and second model, respectively), and the minimum around 99.99 mmHg. On the contrary, in the deformable model the maximum pressure is higher, being 105.25 mmHg, and the minimum pressure lower, being 95.25 mmHg. However, the pressure difference is small in all the cases, and there is no big difference between them.

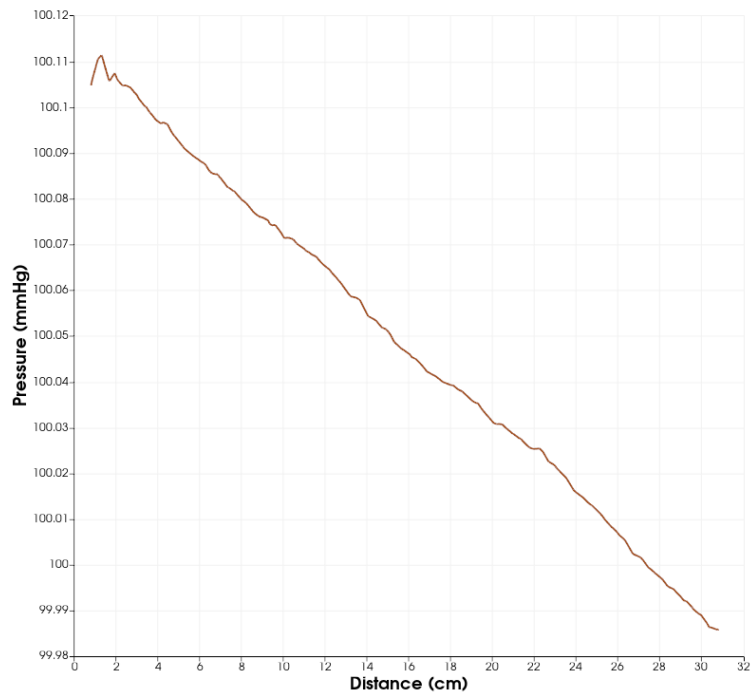
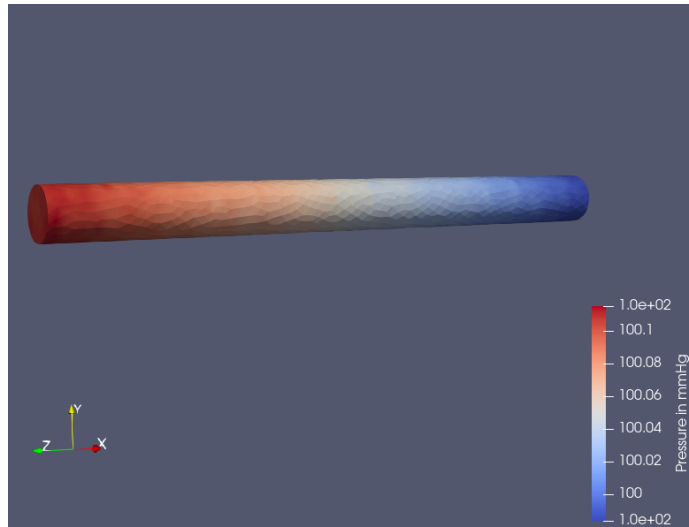


**Figure 29.** Pressure distribution of the first simulation [own source].

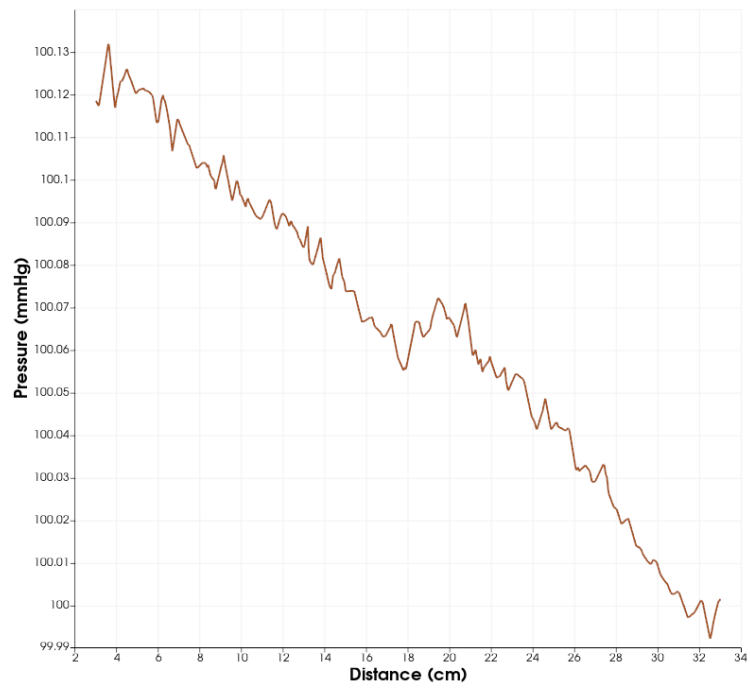
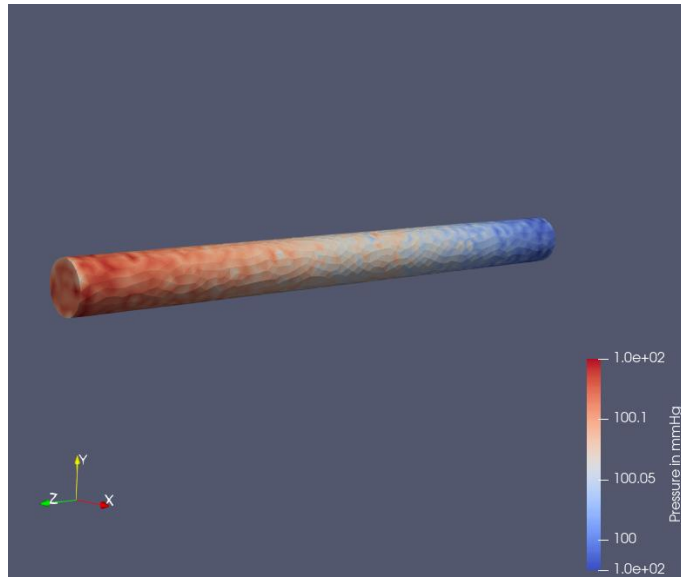


**Figure 30.** Pressure distribution of the second simulation [own source].

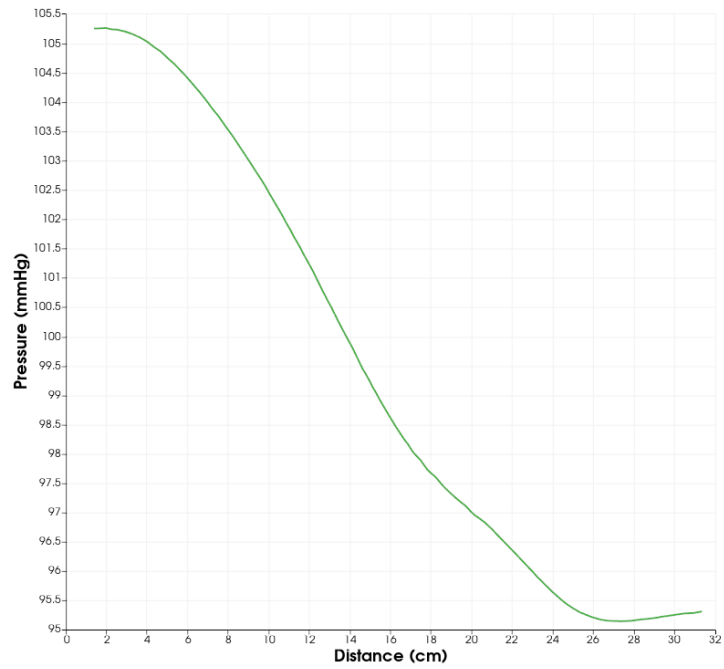
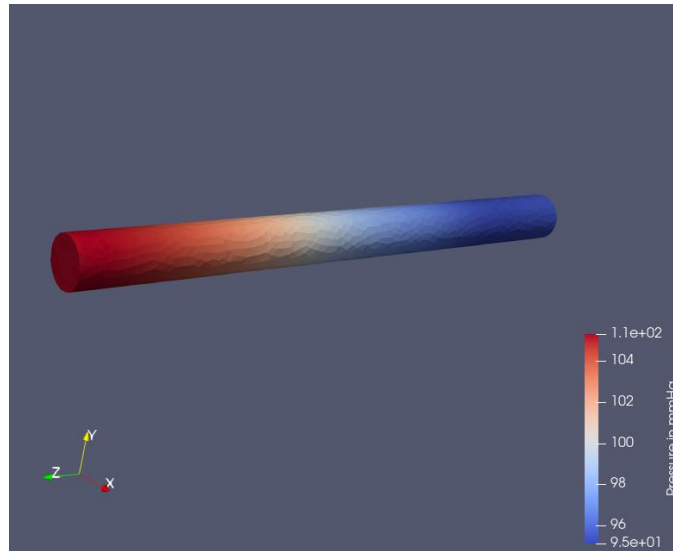


**Figure 31.** Pressure distribution of the third simulation [own source].

Finally, in the deformable model there is also another parameter that can be quantified, which is the displacement. In the rigid models the wall is static, but in the deformable model the fluid deforms the wall. In Figure 32 it can be observed the result of this phenomenon, and the displacement values range is shown. The highest value is 0.35 cm, along all the aortic wall, whereas in the inlet and outlet there is no displacement.

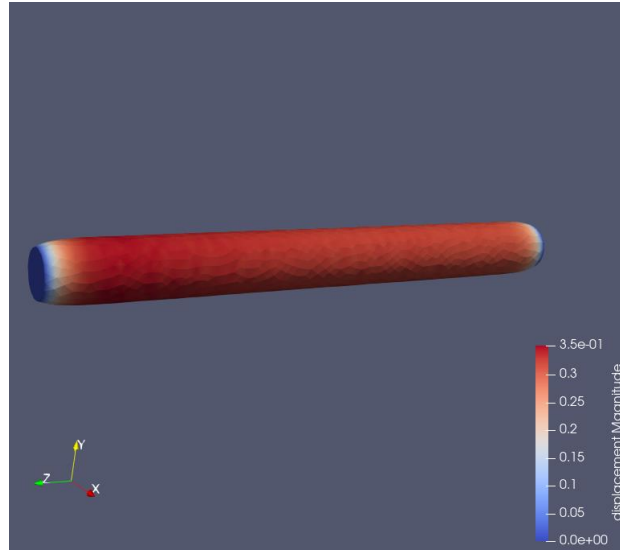


**Figure 32.** Displacement in the deformable model (units: cm) [own source].

To determine if the simulation results are correct, they can be compared with the theoretical results. This can be done for the rigid models using the Hagen – Poiseuille equation (Eq.2), where  $\mu$  is the blood viscosity,  $L$  is the length of the aorta,  $D$  is the diameter of the aorta, and  $\bar{u}$  is the blood mean velocity. This equation gives the pressure drop in an incompressible and Newtonian fluid in laminar flow flowing through a long cylindrical pipe of constant cross section. Therefore, for the last model this law cannot be used because as the wall is deformable the cross section is not constant.

$$\Delta P = \frac{32 \cdot \mu \cdot L}{D^2} \cdot \bar{u} \quad (2)$$

#### Validation of model 1

To evaluate the results of the simulation first the mean velocity ( $\bar{u}$ ) was calculated from the simulation velocity results. The mean velocity can be calculated as half of the maximum velocity, which is 43 cm/s, giving a value of:

$$\bar{u} = \frac{u_{max}}{2} = \frac{43 \text{ cm/s}}{2} = 21.5 \text{ cm/s}$$

Therefore, the theoretical pressure drop will be:

$$\Delta P_{theoretical} = \frac{32 \cdot \mu \cdot L}{D^2} \cdot \bar{u} = \frac{32 \cdot 0.004 \cdot 0.3}{0.025^2} \cdot 0.215 = 13.2 \text{ Pa} = 0.099 \text{ mmHg}$$



From the simulation, it was obtained that the pressure drop is:

$$\Delta P_{simulation} = 100.11 - 99.99 = 0.12 \text{ mmHg}$$

If the error between the theoretical and the obtained value is calculated, the result is:

$$\varepsilon_r = \frac{\Delta P_{simulation} - \Delta P_{theoretical}}{\Delta P_{theoretical}} \cdot 100 = \frac{0.12 - 0.099}{0.099} \cdot 100 = \mathbf{21.2\%}$$

### Validation of model 2

The same procedure was followed for the rigid RCR model. The maximum velocity in this case is 43.5 cm/s, so the mean velocity is:

$$\bar{u} = \frac{u_{max}}{2} = \frac{43.5 \text{ cm/s}}{2} = 21.75 \text{ cm/s}$$

Therefore, the theoretical pressure drop will be:

$$\Delta P_{theoretical} = \frac{32 \cdot \mu \cdot L}{D^2} \cdot \bar{u} = \frac{32 \cdot 0.004 \cdot 0.3}{0.025^2} \cdot 0.218 = 13.4 \text{ Pa} = 0.1 \text{ mmHg}$$

From the simulation, it was obtained that the pressure drop is:

$$\Delta P_{simulation} = 100.12 - 99.99 = 0.13 \text{ mmHg}$$

So, the error between the simulation value and the theoretical value is:

$$\varepsilon_r = \frac{\Delta P_{simulation} - \Delta P_{theoretical}}{\Delta P_{theoretical}} \cdot 100 = \frac{0.13 - 0.1}{0.1} \cdot 100 = \mathbf{30\%}$$

The relative error for both cases is quite big, being 21.2% for the first one and 30% for the second one. As the working scale is very small, any small change results in a large error. There are two reasons that could have caused this difference between the theoretical and simulation values. The first one is that the mesh may haven't been the optimal one. It could be that the mesh wasn't fine enough, making it difficult to correctly capture the gradients and local variations of the pressure, and leading to inaccurate results. The second possible cause is that the flow didn't develop the parabolic profile from the inlet. The distance needed for the fluid to become fully developed after entering a pipe (in this case the aorta) is called hydrodynamic entrance length [57]. Due to viscous forces within the fluid, the layer in contact with the aortic wall has less velocity and slows down the adjacent layers of fluid gradually, forming a velocity profile (Figure 33). Therefore, in this region where the velocity profile is still being developed, the mean velocity is different than the one of the fully developed parabolic profile. As in the formula a single value is taken, this can lead to an error.

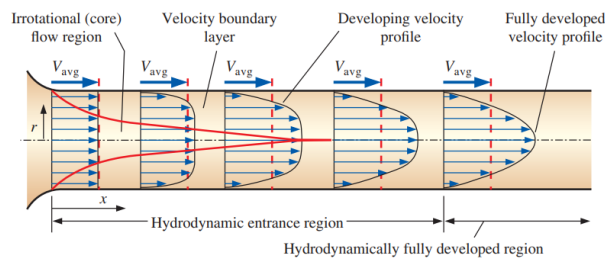


**Figure 33.** Hydrodynamic entrance length. Extracted from [58].

The errors have been calculated considering the flow obtained in the simulation results. However, in the simulation the flow obtained at the inlet was not exactly the same as the one imposed. In the simulation settings, in the inlet boundary condition, it was imposed a flow of 100 cm<sup>3</sup>/s. But in the results a mean velocity of 21.5 cm/s was obtained, and knowing that the radius of the aorta is 1.25 cm, the flow can be calculated as:

$$Q = A \cdot v = \pi \cdot R^2 \cdot v = \pi \cdot 0.0125^2 \cdot 0.215 = 1.055 \cdot 10^{-4} \text{ m}^3/\text{s} = 105.5 \text{ cm}^3/\text{s}$$

Therefore, there is an error between the flow imposed at the inlet and the one that is really obtained. The calculation gives a relative error of 5.5%, which even it is not really big, it would increase the error of the pressure difference if it was made relative to the flow that should have really been at the inlet.

### 5.3.2- Part II

For the second part of the project, the objective was to determine if the aortic dissection patch would imply an improvement with respect to the actual treatment for aortic dissection, the stent graft (TEVAR). To prove it, the pressure waveforms were obtained from the transient simulations of every model.

In Figure 34 is shown the proximal pressure waveform obtained for the healthy aorta model. It can be observed that the result obtained is similar to the real pressure waveform of the aorta (Figure 35). It is clearly represented the first wave (systole), corresponding to the waveform going from the inlet to the outlet, and the second wave (diastole), corresponding to the return waveform, as well as the dicrotic notch between them. However, in Figure 34 it is present a small third wave, which should not be present in a normal aortic pressure waveform. This could be due to the dynamic response of the vessel: the pressure pulse deforms the vessel and at the same time this deformation affects the pressure pulse, causing oscillations until reaching equilibrium. Probably in reality there are some external factors that attenuate these oscillations, which have not been considered in this model.

Regarding the pressure values obtained, it can be observed that the systolic peak is at 13,048.5 Pa (97.9 mmHg) and the diastolic peak is at 11,732.1 Pa (88 mmHg). The systolic pressure is inside the normal range of systolic arterial pressure (>90 mmHg and <120 mmHg), whereas the diastolic blood pressure is higher than the normal one, reaching hypertension values (>80 mmHg) according to the American blood pressure classification [59, 60, 61]. This high diastolic pressure could be due to the small deformation of the aortic wall, which is only displaced 0.32 mm (Figure 36). As there is a small deformation, the pressure is not damped enough, so it returns with a higher value than the normal one.

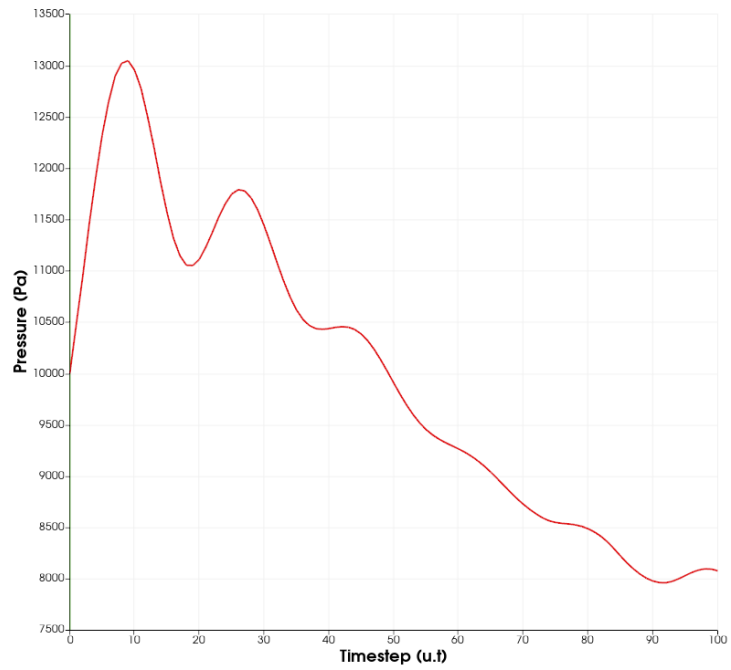


Figure 34. Proximal pressure waveform of the simulated healthy aorta [own source].

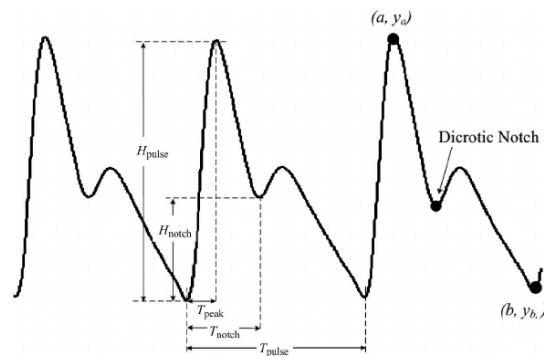


Figure 35. Reference pressure waveform of the healthy aorta. Extracted from [62].

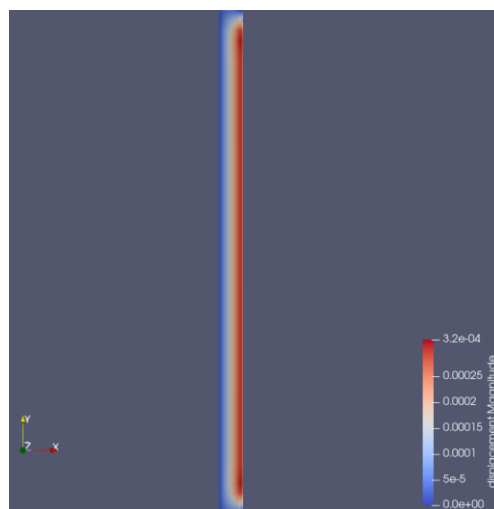


Figure 36. Displacement of the healthy aortic wall (units: m) [own source].

In Figure 37 is shown the proximal pressure waveform obtained for the aortic dissection model with the stent graft. In order to compare it with the model of the healthy aorta (Figure 34), the second peak has to be analyzed because the first one is the generated pulse, that should be the same (or very similar) in all the models, whereas the second one is the return pulse, which has experienced the effect of all the materials. If both figures are compared, it can be verified that the first peak has a similar amplitude, with a value of 13,048.5 Pa (97.9 mmHg) in the healthy aorta model and a value of 13,132.4 Pa (98.5 mmHg) in the stent graft model. This variation could be because the geometry changes with the deformation, which is different depending on the properties of the materials, making that the resistance is different and therefore, that the pressure slightly varies.

Regarding the second peak, it can be observed that the amplitude is 11,732.1 Pa (88 mmHg) in the healthy aorta model and 11,977.4 Pa (89.8 mmHg) in the stent graft model. Due to the variations in the systolic pressure, to compare both models the difference between the systolic and the diastolic pressure will be compared. The pressure difference for the healthy aorta model is 1,316.4 Pa (9.9 mmHg) and for the stent graft model is 1,155 Pa (8.7 mmHg).

Several studies have demonstrated that stent grafts implanted in the aorta can affect the natural elasticity of the vessel wall. The aorta is responsible for dampening the pulsatile pressure generated by the heart, but if the stent graft causes the aortic wall to become stiffer, it may result in increased pressure within the arterial system, leading to hypertension [63]. Therefore, the pressure waveform of the aorta should have a lower pressure due to the dampening effect, whereas the one of the stent graft model should be higher due to the rigidity of the stent, that reduces this effect. This is what can be observed in the results obtained, where the diastolic peak is higher in the stent graft model than in the healthy aorta model. If the pressure difference is analyzed, it can be observed that it is smaller in the stent graft model, because the pressure of the return pulse (diastolic) is more similar to the pressure of the generated pulse (systolic), as the pressure is practically not damped. However, the changes between both models are small, which could be because there is a small deformation of the aortic wall (0.32 mm), as it can be observed in Figure 36.

Another variable that can be studied is the velocity of the pulse, which can be analyzed by looking at the time when the peak is reached. If both graphs are compared, it can be observed that the pressure waveform returns before in the stent graft model than in the healthy aorta model. The pulse wave velocity (PWV) can be described by the Moens – Korteweg equation (Eq.3):

$$PWV = \sqrt{\frac{E_{inc} \cdot h}{2 \cdot r \cdot \rho}} \quad (3)$$

Where  $E_{inc}$  is the incremental elastic modulus (distensibility of the artery),  $h$  is the wall thickness,  $r$  is the vessel radius and  $\rho$  is the blood density. Therefore, the velocity of the pulse is related with the elastic modulus. This explains why the pulse is faster in the stent graft model because as the stent graft has a larger elastic modulus (more rigid) than the aortic wall, it has a greater PWV, and the peak is reached before.

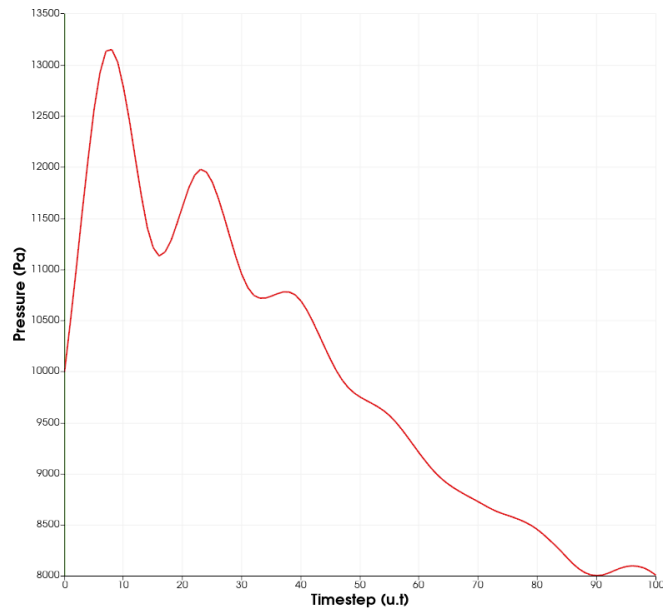


**Figure 37.** Proximal pressure waveform of the aortic dissection with the stent graft [own source].

For now, it has been discussed the results obtained for the healthy aorta model and the stent graft model. However, the main goal was to determine the response of the patch. In Figure 38 it can be observed the proximal pressure waveform obtained for the aortic dissection model with the patch. The systolic pressure has a value of 12,921 Pa (96.9 mmHg), being lower than in the other models.

The diastolic pressure is also lower, obtaining a value of 11,569.6 Pa (86.8 mmHg). The value should be similar than the one of the healthy aorta because the patch has similar mechanical properties. The pressure difference with respect to the first peak is 1,351.4 Pa (10.1 mmHg), so there is a larger variation between the pressure of the generated pulse and the pressure of the return pulse in comparison with the healthy aorta. This difference could be because the part of the aortic dissection is more flexible and it is more deformed, dampening more the pressure pulse and causing a decrease in the amplitude of the return pulse (diastolic pressure).

Regarding the velocity of the pulse, it can be observed that in the patch model it travels more slowly than in the stent graft and healthy aorta models because the peaks are produced slightly after, especially the second peak that is almost at 30 u.t (0.15 s). As mentioned before, the pulse velocity is related with the elastic modulus. As in the patch model the part of the aortic dissection has a smaller elastic modulus than the healthy aortic wall, the pressure waveform velocity is decreased.

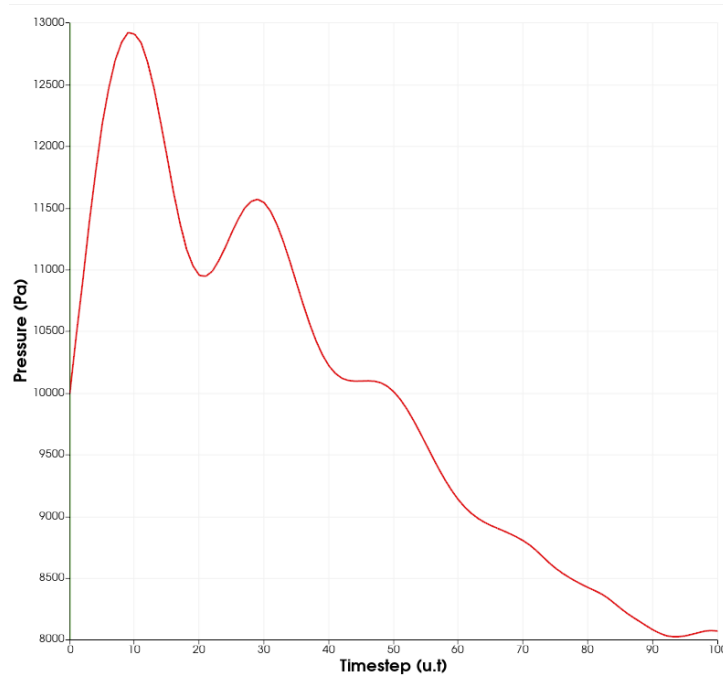


**Figure 38.** Proximal pressure waveform of the aortic dissection with the patch [own source].

## 6. Execution chronogram

### 6.1- Work-breakdown structure (WBS)

In this section the work-breakdown structure of the project will be reviewed. The project is divided into different sections that englobe the steps that have been carried out during the development of the project (Figure 39).

The first one is the project management, that involves all the steps previous to the start of the practical part of the project, like the objective's definition, the research of the state of the art, the market analysis and the tasks organization.

The second one refers to the first part of the practical part of the project (Part I), which is the modelling and simulation of the healthy aorta and the aortic dissection, followed by the analysis of results. In this case, the modelling and simulation of the aortic dissection with the patch hasn't been included because as the simulations with the aortic dissection didn't work, it couldn't be performed, and it was moved on to the second part.

The third one refers to the second part of the practical part of the project (Part II), which is the modelling and simulation of the healthy aorta, the aortic dissection with the stent graft, and the aortic dissection with the patch, concluding with the analysis of results.

The last one is the report and presentation, which refers to the writing of the report and the preparation of the presentation that had to be performed in parallel and after the realization of the practical part.

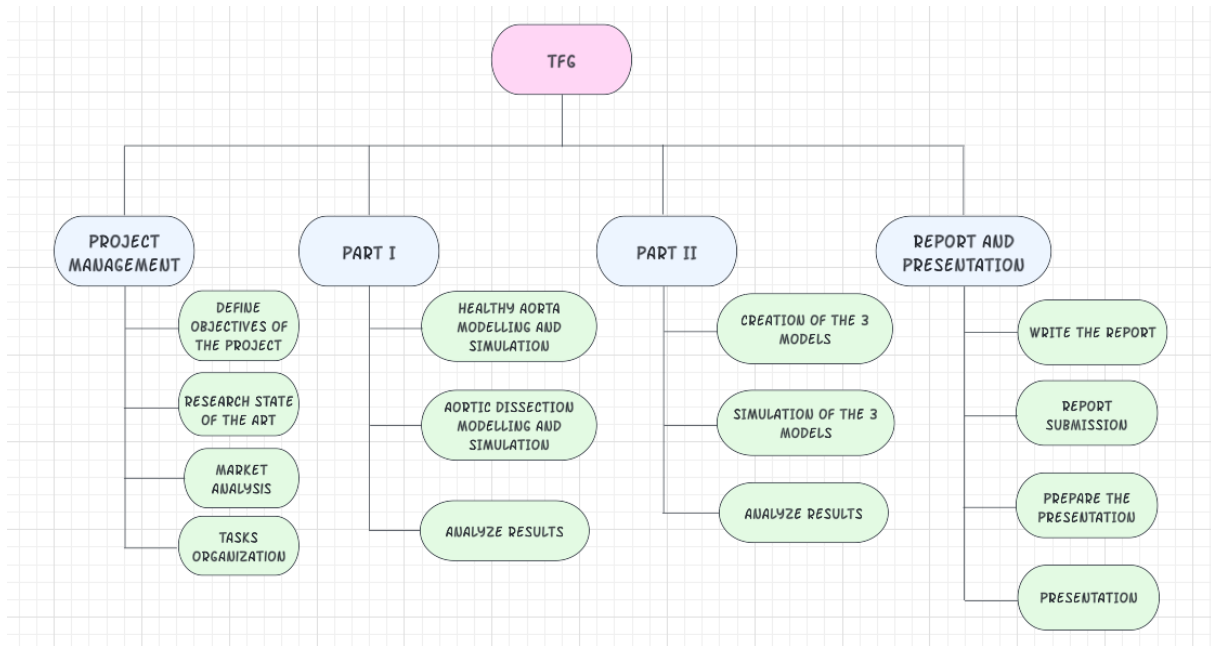


**Figure 39.** Work-breakdown structure of the project [own source].

## 6.2- Gantt chart

The execution chronogram was followed as shown in the Gantt chart (Figure 40). As previously mentioned, there were some obstacles during the development of the project, which caused a change in the initial planning. Initially, the aortic dissection modelling and simulation would have taken more time and instead of the second part of the project there would be the modelling and simulation of the aortic dissection with the patch, followed by the analysis of results. However, this is not shown in the Gantt chart because it was not possible to reach this stage, so the first part of the project (Part I) had to be abandoned. Consequently, another direction was taken for the project, which led to the second part of the project that is shown in the Gantt chart (Part II).

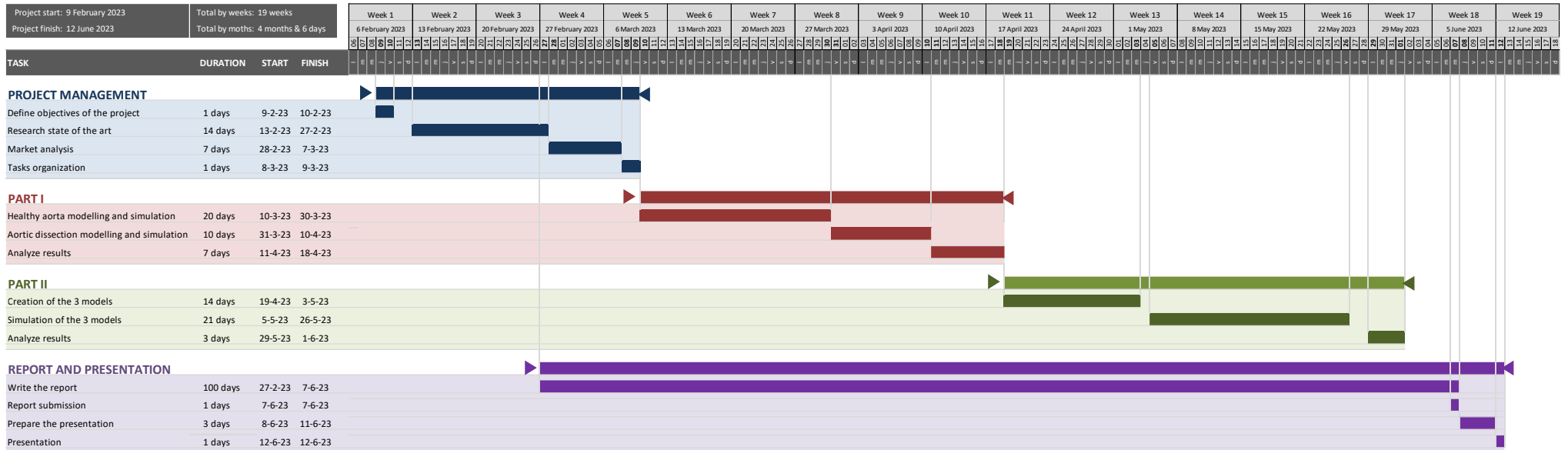


Figure 40. Gantt chart of the project [own source].



## 7. Technical viability

The technical viability of the project will be determined using the SWOT analysis (Table 11). The internal factors (strengths and weaknesses) and the external factors (opportunities and threats) that affect the project will be assessed.

**Table 11.** SWOT analysis of the project.

<b>Strengths</b>	<b>Weaknesses</b>
<ul style="list-style-type: none"> <li>• Collaboration with CIMNE and UB.</li> <li>• Axisymmetric models.</li> <li>• Model dimensions and mesh can be easily modified.</li> <li>• Open-source software.</li> <li>• Offers an alternative to animal experimentation.</li> </ul>	<ul style="list-style-type: none"> <li>• Ideal model.</li> <li>• No similar studies performed using Elmer.</li> <li>• Elmer is a limited software for cardiovascular simulations.</li> <li>• No prior experience with FEM simulations.</li> </ul>
<b>Opportunities</b>	<b>Threats</b>
<ul style="list-style-type: none"> <li>• Increasing need for medical device testing and fabrication.</li> <li>• Collaboration with medical device companies.</li> </ul>	<ul style="list-style-type: none"> <li>• There are other research groups making similar studies.</li> <li>• Regulations may limit the study capabilities.</li> </ul>

### 7.1- Strengths

One of the strengths of this project is that it was developed in collaboration with CIMNE and UB, so the author could count on two researchers specialized in the subject to help her face the problems encountered during the project. Going into more technical aspects, another strength is the use of axisymmetric models, which reduces the computational time required to run the simulations, so it offers a more rapid obtention of the results. In addition, as the models are created from a .geo file code, they are easily modifiable because it is just needed to modify the values of the parameters and the model will be redesigned. The same happens with the mesh size because to change it the number of layers of the code can be changed, consequently modifying the mesh size. Another strength is that an open-source software has been used, therefore reducing the costs needed for the project. Finally, it is important to mention that by using these *in silico* models and testing them in physiological conditions, the animal experimentation can be avoided or reduced.

### 7.2- Weaknesses

The main weakness of the project is that the simulations are performed with ideal models. To have more realistic results the models should be patient-specific, created from the segmentation of CTA images. Therefore, it has to be considered that the geometry of the models created is not exactly the same as a real aorta. Another weakness is that there are no other FEM studies of aortic dissection performed with Elmer, which could be because it's not the most appropriate program to use. One of the weaknesses of Elmer regarding the application of this project is that it's not specific for biomechanical simulations, so not all the conditions present in the cardiovascular system can

be represented. Another important weakness of this project is that the author had no prior experience with FEM simulations, which difficulted the problems faced during the development of the project.

### 7.3- Opportunities

The medical device industry is constantly growing, however an important limitation when it comes to the commercialization of the devices in the market is that the regulations in the healthcare sector are very strict. The companies have to go through animal studies and several clinical trials before obtaining the approval to launch it to the market. The use of FEM simulations can accelerate this process by predicting the expected result in a real scenario, decreasing the number of tests needed before approval. Therefore, this means that there is a large market that would be interested in the content developed in this project. Another opportunity for this project is the collaboration with medical device companies, such as Aortyx, as the project is based on validating the performance of the medical device. Therefore, they could be interested in this project and its continuation.

### 7.4- Threats

One of the threats that could face this project is that there are other research groups making similar studies and with more experience in the field, that could be our competitors. Another threat is the regulations because any change or new condition can limit the study capabilities.

## 8. Economic viability

In this section, the estimated costs of the project are presented (Table 12). The costs have been divided into three categories: human resources, software, and hardware. For each category, there are listed the different items that are included, and it is shown the cost per unit, quantity, and total cost of each item. At the bottom, the overall cost of the project is presented.

**Table 12.** Breakdown of the estimated costs of the project.

	Item	Cost per unit	Quantity	Total cost
Human resources	Student salary	12.95€/h	300h	3,885€
	Supervisor CIMNE UPC salary	17.63€/h	50h	881.5€
	Supervisor UB salary	16.51€/h	50h	825.5€
Software	Gmsh	0€	1 license	0€ (open-source)
	GiD	0€	1 license	0€ (open-source)
	SimVascular	0€	1 license	0€ (open-source)
	Elmer	0€	1 license	0€ (open-source)
	ParaView	0€	1 license	0€ (open-source)
Hardware	Laptop	700€	1 unit	700€
<b>TOTAL</b>				<b>6,292€</b>

First of all, regarding the **human resources**, it has been considered the salary of the student as the mean salary of a junior biomedical engineer, which is of 29,000€ per year [64]. Considering that the annual salary is distributed in 14 payments, the monthly salary is of 2,071.43€, which corresponds to 12.95€/h assuming a workday of 8h. As the final degree project is expected to be carried out in 300h, the total cost of the student is 3,885€. The salary of the supervisor at CIMNE UPC is 2,820.54€/month (17.63€/h) because it is the standard salary of a research director in UPC [65]. The supervisor at UB is an associate professor, and the corresponding salary is 2,642.27€/month (16.51€/h), which can be found in the Portal of Transparency of the university

[66]. The supervisors dedicate less time to the project than the student, so a time of 50h has been estimated. Therefore, the total salary for the supervisor at CIMNE will be 881.5€ and the total salary for the supervisor at UB will be 825.5€. The sum of both gives a total of 1,707€ for the human resources cost.

The project has been performed using different modelling and simulation programs, which are included in the **software** category. The programs used are Gmsh, GiD, SimVascular, Elmer and ParaView. All these programs are open source and can be downloaded freely, therefore they have a cost of 0€.

Finally, it has been considered in the **hardware** category the cost of the laptop that has been used for the project, which is an HP 340S G7 Notebook and had a cost of 700€.

As it can be observed in Table 12, the **overall cost** of the project is 6,292€.

## 9. Regulation and legal aspects

This project has been developed in Spain, so it must fulfil the legal requirements of the Spanish legislation. As it is the final degree project of the bachelor's degree in biomedical engineering, it has to follow the regulations of the final degree project of the University of Barcelona, which are the "*Normes generals reguladores dels treballs de fi de grau de la Universitat de Barcelona*" and the "*Normes reguladores des treballs de fi de grau en enginyeria biomèdica*" [67, 68].

The FEM software programs used in the development of the project cannot be considered a medical device as they don't follow the medical device definition established in the section 201(h) of the FDA [69]:

*An instrument, apparatus, implement, machine, contrivance, implant, in vitro reagent, or other similar or related article, including a component part or accessory which is:*

- *(A) recognized in the official National Formulary, or the United States Pharmacopoeia, or any supplement to them,*
- *(B) intended for use in the diagnosis of disease or other conditions, or in the cure, mitigation, treatment, or prevention of disease, in man or other animals, or*
- *(C) intended to affect the structure or any function of the body of man or other animals, and which does not achieve its primary intended purposes through chemical action within or on the body of man or other animals and which does not achieve its primary intended purposes through chemical action within or on the body of man or other animals and which is not dependent upon being metabolized for the achievement of its primary intended purposes. The term "device" does not include software functions excluded pursuant to section 520(o).*

Therefore, they don't need to follow the legislation and regulation of medical devices. However, the FDA has established guidelines for the use of computational modelling and simulations in medical device development. The aim of these guidelines is to ensure that the simulations are accurate, reliable, and validated properly.

The guidelines recommend that the following steps are followed:

1. **Develop a simulation plan:** the plan should describe the purpose of the simulation, the assumptions and limitations, the inputs and outputs, and the methods that will be used to validate it.
2. **Select appropriate modelling techniques:** the modelling techniques should accurately represent the geometry, material properties and conditions of the medical device.
3. **Validate the simulation:** the simulation should be validated by comparing the simulation data to experimental data or other validated results. The validation should demonstrate that the simulation accurately predicts the behaviour of the device under different conditions.
4. **Document the simulation:** the simulation results and methods used to perform the simulation should be documented in detail.
5. **Use the simulation to support regulatory submissions:** the simulation results can be used to support regulatory submissions to the FDA. The results should be presented in a clear and concise manner and should be supported by appropriate documentation.

## 10. Conclusions

In conclusion, this project highlighted the potential of FEM simulations to test medical devices for cardiovascular applications and analyze their performance in biological conditions before being implanted. FSI simulations are very useful to solve fluidic mechanical problems, which is especially important in cardiovascular problems, as the behaviour of both the vessel wall and the blood flow is considered.

The aortic dissection is a complex disease, which has led to some complications for the modelling and simulation. It can be concluded that SimVascular is not the best program to perform simulations with ideal models. Although it allows the importation of CAD models, the software was designed for patient-specific simulations, to make the models from real images following the established pipeline. The validation of the results obtained in SimVascular for the healthy aorta model showed that the error between the simulation results and the theoretical value was too large. In the future, more tests should be performed with different mesh sizes until the optimal is found. In addition, the entrance length should be calculated, and the length of the aorta could be increased to account for this variable, so that the pressure difference is calculated with already a parabolic velocity profile for the whole length of the aorta.

Regarding the comparison between the stent graft and the aortic patch, it has been observed that the pressure of the model with the patch is closer to the one of the healthy aorta than the stent graft, which is higher. However, as with the healthy model there is already hypertension and the difference between the models is small, it cannot be confirmed that the patch is a better option than the stent graft to avoid causing hypertension in the aortic dissection treatment. The reason of this hypertension in the healthy aorta could be because of the little wall displacement, which caused that the pressure wasn't damped enough. The value of the Young's modulus of the aortic wall has been found to be quite variable across different studies. Therefore, a smaller Young's modulus could be used to have a more elastic wall. However, probably a software different than Elmer should be used because with Elmer it was discovered that, if the Young's modulus is of an order smaller than MPa, the simulations don't converge.

Finally, from a future perspective, it would be interesting to make these simulations with patient-specific models. Due to the short time that we had to develop the project, the scope was limited to ideal models. However, to obtain more realistic and accurate results, CTA images from real patients should be used to make the model and, in this case, probably SimVascular would be more appropriate to make the simulations.

## 11. References

- [1] R. Zorrilla, E. Soudah, and R. Rossi, "Computational modeling of the fluid flow in type B aortic dissection using a modified finite element embedded formulation," *Biomech. Model Mechanobiol.*, vol. 19, no. 5, pp. 1565–1583, Oct. 2020.
- [2] C. A. Nienaber, R. E. Clough, N. Sakalihasan *et al.*, "Aortic dissection," *Nature Reviews Disease Primers*, vol. 2, no. 1, pp. 1–18, Jul. 2016.
- [3] T. Gudbjartsson, A. Ahlsson, A. Geirsson *et al.*, "Acute type A aortic dissection – a review," *Scandinavian Cardiovascular Journal*, vol. 54, no. 1, pp. 1–13, Jan. 2019.
- [4] C. W. Chen Y.H. Tseng, C.C. Lin *et al.*, "Aortic dissection assessment by 4D phase-contrast MRI with hemodynamic parameters: the impact of stent type," *Quant. Imaging Med. Surg.*, vol. 11, no. 2, pp. 490-501, Feb. 2021.
- [5] G. Soulat, P. McCarthy, and M. Markl, "4D Flow with MRI," *Annual Review of Biomedical Engineering*, vol. 22, pp. 103–126, Jun. 2020.
- [6] M. Bashir, M. Jubouri, R. Patel *et al.*, "Cost Analysis of Thoracic Endovascular Aortic Repair in Type B Aortic Dissection: How Much Does Quality Cost?," *Ann. Vasc. Surg.*, Oct. 2022. doi: 10.1016/j.avsg.2022.09.043.
- [7] M.A. Farber and F.E Parodi, "Aortic Dissection" in *MSD Manual Professional Edition*. [Online]. Available: <https://www.msmanuals.com/professional/cardiovascular-disorders/diseases-of-the-aorta-and-its-branches/aortic-dissection>
- [8] F. Jordan, B. Fitzgibbon, E. Kavanagh, *et al.*, "Endovascular versus open surgical repair for complicated chronic Type B aortic dissection," *Cochrane Database Syst Rev*, vol. 12, no. 12, Dec. 2021, Art. no. CD012992.
- [9] K.R. Ahmed, P. Pathmanathan, S.V. Kabadi, *et al.*, "Successes and Opportunities in Modeling & Simulation for FDA" U.S. Food and Drug Administration, Silver Spring, Maryland, USA, Nov. 2022. [Online]. Available: <https://www.fda.gov/science-research/about-science-research-fda/modeling-simulation-fda>
- [10] E. Soudah, "Computational fluid dynamics indicators to improve cardiovascular pathologies", Ph.D. Thesis, Dept. Chemical Engineering, UPC, Barcelona, Spain, 2016. [Online]. Available: <http://hdl.handle.net/2117/96285>
- [11] E. Soudah, R. Rossi, S. Idelsohn *et al.*, "A reduced-order model based on the coupled 1D-3D finite element simulations for an efficient analysis of hemodynamics problems", *Comput. Mech.*, vol. 54, pp.1013–1022, Oct. 2014.
- [12] S. Bonilla and E. Soudah, "Uso de analogías eléctricas para entender patologías cardiovasculares", Monograph CIMNE (2018). M182 [Online]. Available: [https://www.scipedia.com/public/Bonilla\\_et\\_al\\_2019aSoudah\\_Prieto,\\_E.\\_\(2016\)](https://www.scipedia.com/public/Bonilla_et_al_2019aSoudah_Prieto,_E._(2016)).

- [13] E. Soudah, E. Y. K. Ng, T. H. Loong, M. Bordone, U. Pua, and S. Narayanan, "CFD modelling of abdominal aortic aneurysm on hemodynamic loads using a realistic geometry with CT," *Computational and Mathematical Methods in Medicine*, vol. 2013, Jun. 2013, Art. no. ID 472564.
- [14] R. Thomas, "Improving Medical Devices Using Computational Modeling", The American Society of Mechanical Engineers (ASME) New York, NY, USA. Feb. 13, 2012. [Online]. Available: <https://www.asme.org/topics-resources/content/improving-medical-devices-using-computational-mode>
- [15] P. Ryzhakov, E. Soudah, and N. Dialami, "Computational modeling of the fluid flow and the flexible intimal flap in type B aortic dissection via a monolithic arbitrary Lagrangian/Eulerian fluid-structure interaction model," *Int. J. Numer. Method. Biomed. Eng.*, vol. 35, no. 11, Nov. 2019, Art. no. e3239.
- [16] E. Soudah, P. Rudenick, M. Bordone, *et al.*, "Validation of numerical flow simulations against in vitro phantom measurements in different type B aortic dissection scenarios," *Computer Methods in Biomechanics and Biomedical Engineering*, vol. 18, no. 8, pp. 805–815, Jun. 2014.
- [17] K. Bäumlér, V. Vedula, A.M. Sailer *et al.*, "Fluid–structure interaction simulations of patient-specific aortic dissection," *Biomech. Model Mechanobiol.*, vol. 19, no. 5, pp. 1607–1628, Oct. 2020.
- [18] Y. Zhu, S. Mirsadraee, U. Rosendahl, J. Pepper, and X. Y. Xu, "Fluid-Structure Interaction Simulations of Repaired Type A Aortic Dissection: a Comprehensive Comparison With Rigid Wall Models," *Front. Physiol.*, vol. 13, Jun. 2022, Art. no. 913457.
- [19] L. Weltert, R. De Paulis, R. Scaffa, D. Maselli, A. Bellisario, and S. D'Alessandro, "Re-creation of a sinuslike graft expansion in Bentall procedure reduces stress at the coronary button anastomoses: A finite element study," *Journal of Thoracic and Cardiovascular Surgery*, vol. 137, no. 5, pp. 1082–1087, May 2009.
- [20] D. Marlevi, J.A. Sotelo, R. Grogan-Kaylor *et al.*, "False lumen pressure estimation in type B aortic dissection using 4D flow cardiovascular magnetic resonance: comparisons with aortic growth," *Journal of Cardiovascular Magnetic Resonance*, vol. 23, no. 1, Dec. 2021, Art. no. 51.
- [21] Y. Zhu, X. Y. Xu, U. Rosendahl, J. Pepper, and S. Mirsadraee, "Advanced risk prediction for aortic dissection patients using imaging-based computational flow analysis", *Clin. Radiol.*, vol.78, no. 3, pp. e155-e165, Mar. 2023.
- [22] P. A. Rudenick, B. H. Bijnens, D. García-Dorado, and A. Evangelista, "An in vitro phantom study on the influence of tear size and configuration on the hemodynamics of the lumina in chronic type B aortic dissections," *J. Vasc. Surg.*, vol. 57, no. 2, pp. 464-474.e5, Feb. 2013.



- [23] C. H. Armour, B. Guo, S. Saitta *et al.*, "Evaluation and verification of patient-specific modelling of type B aortic dissection," *Comput. Biol. Med.*, vol. 140, Jan. 2022, Art. no. 105053
- [24] X. Li, H. Qiao, Y. Shi *et al.*, "Role of proximal and distal tear size ratio in hemodynamic change of acute type A aortic dissection," *J. Thorac. Dis.*, vol. 12, no. 6, pp. 3200-3210, Jun. 2020.
- [25] C. J. Mills, I.T. Gabe, J.H. Gault *et al.*, "Pressure-flow relationships and vascular impedance in man," *Cardiovasc. Res.*, vol. 4, no. 4, pp. 405–417, Oct. 1970.
- [26] M. S. Olufsen, C. S. Peskin, W. Y. Kim, E. M. Pedersen, A. Nadim, and J. Larsen, "Numerical Simulation and Experimental Validation of Blood Flow in Arteries with Structured-Tree Outflow Conditions," *Ann. Biomed. Eng.*, vol. 28, pp.1281-1299, Nov. 2000.
- [27] Y. Hohri, S. Numata, K. Itatani *et al.*, "Prediction for future occurrence of type A aortic dissection using computational fluid dynamics," *European Journal of Cardio-Thoracic Surgery*, vol. 60, pp. 384–391, Feb. 2021.
- [28] M. Y. Chong, B. Gu, C. H. Armour *et al.*, "An integrated fluid-structure interaction and thrombosis model for type B aortic dissection," *Biomech. Model Mechanobiol.*, vol. 21, pp. 261–275, Feb. 2022.
- [29] M. Y. Chong, B. Gu, B. T. Chan, Z. C. Ong, X. Y. Xu, and E. Lim, "Effect of intimal flap motion on flow in acute type B aortic dissection by using fluid-structure interaction," *Int. J. Numer. Method Biomed. Eng.*, vol. 36, no. 12, Dec. 2020, Art. no. e3399.
- [30] H. Xu, M. Piccinelli, B. G. Leshnower, A. Lefieux, W. Robert Taylor, and A. Veneziani, "Coupled Morphological-Hemodynamic Computational Analysis of Type B Aortic Dissection: A Longitudinal Study," *Annals of biomedical engineering*, vol.47, no.7, pp.927-939, Jul. 2018.
- [31] Z. Cheng, F.P. Tan, C.V. Riga *et al.*, "Analysis of flow patterns in a patient-specific aortic dissection model," *J. Biomech. Eng.*, vol. 132, no. 5, May 2010.
- [32] Z. Cheng, C. Juli, N. B. Wood, R. G. J. Gibbs, and X. Y. Xu, "Predicting flow in aortic dissection: Comparison of computational model with PC-MRI velocity measurements," *Med. Eng. Phys.*, vol. 36, no. 9, pp. 1176–1184, Sep. 2014.
- [33] D. Dillon-Murphy, A. Noorani, D. Nordsletten, and C. A. Figueroa, "Multi-modality image-based computational analysis of haemodynamics in aortic dissection" *Biomech. Model Mechanobiol.*, vol. 15, no. 4, pp. 857-876, Aug. 2016.
- [34] K. C. Wang, R. W. Dutton, and C. A. Taylor, "Improving geometric model construction for blood flow modeling: Geometric image segmentation and image-based model construction for computational hemodynamics," *IEEE Engineering in Medicine and Biology Magazine*, vol. 18, no. 6, pp. 33–39, Nov. 1999.

- [35] T. Luebke and J. Brunkwall, "Type B Aortic Dissection A Review of Prognostic Factors and Meta-analysis of Treatment Options", *Aorta (Stamford)*, vol.2, no.6, pp.265-78, Dec. 2014.
- [36] R. S. McClure, S. B. Brogly, K. Lajkosz *et al.*, "Economic Burden and Healthcare Resource Use for Thoracic Aortic Dissections and Thoracic Aortic Aneurysms—A Population-Based Cost-of-Illness Analysis," *Journal of the American Heart Association: Cardiovascular and Cerebrovascular Disease*, vol. 9, no. 11, Jun. 2020, Art. no. e014981.
- [37] A. Mathlouthi, B. Nejm, G. A. Magee, J. J. Siracuse, and M. B. Malas, "Hospitalization Cost and In-hospital Outcomes Following Type B Thoracic Aortic Dissection Repair," *Ann. Vasc. Surg.*, vol. 75, pp. 22–28, Aug. 2021.
- [38] *Autocad*. (2023). Autodesk Inc. Available: <https://www.autodesk.es/products/autocad/free-trial>
- [39] C. Geuzaine, J.-F. Remacle (distributed under the terms of the GNU General Public License). *Gmsh 4.11.1*. (2022). Release: Dec. 21, 2022. Available. <http://gmsh.info/>
- [40] *GiD 16.0.5*. (2023). Release: May 30, 2023. International Center for Numerical Methods in Engineering (CIMNE). Available: <https://www.gidhome.com/>
- [41] *Ansys*. (2023). Release. Ansys Inc. Available: <https://www.ansys.com/>
- [42] C.A. Figueroa, M. Marcan, R. Khlebnikov, et al. *CRIMSON*. (2022). CRIMSON Technologies LLC. Available: <http://www.crimson.software/>
- [43] *SimVascular*. (2023). Release: May 24, 2023. SimVascular Development Team. Available: <https://simvascular.github.io/>
- [44] P. Dadvand, R. Rossi. *Kratos Multiphysics*. (2023). CIMNE (International Center for Numerical Methods in Engineering) Available: <https://github.com/KratosMultiphysics/Kratos>
- [45] P. Dadvand, R. Rossi, and E. Oñate, "An object-oriented environment for developing finite element codes for multi-disciplinary Applications", *Arch. Comput. Methods Eng.*, vol. 17, no. 3, p.253–297, Sep. 2010.
- [46] *Elmer FEM v.8.4*. (2019). Release: Ap. 9, 2019. CSC – IT Center For Science LTD. Available: <http://www.elmerfem.org/blog/>
- [47] *ParaView*. (2023). Release: 5.11.0. Kitware Inc. Available: <https://www.paraview.org/>
- [48] G. Sendić, "Aorta", Kenhub GmbH, Leipzig, Germany, Nov. 23, 2022. [Online]. Available: <https://www.kenhub.com/en/library/anatomy/aorta>
- [49] S. Prieto-González, P. Arguis, A. García-Martínez *et al.*, "Large vessel involvement in biopsy-proven giant cell arteritis: prospective study in 40 newly diagnosed patients using CT angiography," *Ann. Rheum. Dis.*, vol. 71, no. 7, pp. 1170–1176, Jul. 2012.

- [50] C. J. Beller, M. R. Labrosse, M. J. Thubrikar, and F. Robicsek, "Finite element modeling of the thoracic aorta: including aortic root motion to evaluate the risk of aortic dissection," *Journal of medical engineering & technology*, vol. 32, no. 2, pp. 167–170, Mar. 2009.
- [51] N. M. Pahlevan and M. Gharib, "Aortic Wave Dynamics and Its Influence on Left Ventricular Workload," *PLoS One*, vol. 6, no. 8, Aug. 2011, Art. no. e23106.
- [52] "Endovascular stent graft for aortic dissection", UpToDate, Inc, Wolters Kluwer, Alphen aan den Rijn, Netherlands. [Online]. Available: <https://www.uptodate.com/contents/image?imageKey=PI%2F84002>
- [53] J. Tambaca, S. Canic, M. Kosor, R. D. Fish, and D. Paniagua, "Mechanical behavior of fully expanded commercially available endovascular coronary stents", *Tex. Heart Inst. J.*, vol.38, no.5, pp.491-501, 2011.
- [54] "Density of Stainless Steel", thyssenkrupp Materials (UK) Ltd., Cradley Heath, West Midlands, UK. [Online]. Available: <https://www.thyssenkrupp-materials.co.uk/density-of-stainless-steel>.
- [55] Y. Zhu, S. Mirsadraee, U. Rosendahl, J. Pepper, and X. Y. Xu, "Fluid-Structure Interaction Simulations of Repaired Type A Aortic Dissection: a Comprehensive Comparison With Rigid Wall Models," *Front. Physiol.*, vol. 13, Jun. 2022, Art. no. 913457.
- [56] M. Catanho, M. Sinha, and V. Vijayan, "BENG 221-Mathematical Methods in Bioengineering Model of Aortic Blood Flow Using the Windkessel Effect", Oct. 25, 2012. [Online]. Available: <https://www.semanticscholar.org/paper/Model-of-Aortic-Blood-Flow-Using-the-Windkessel-Catanho-Sinha/93b6289654477c49b0d0ba07ed08922e05e87a4a>
- [57] R. K. Shah and A. L. London, "Dimensionless Groups and Generalized Solutions" in *Laminar Flow Forced Convection in Ducts*, Editors: T. Irvine and J.P. Hartnett, Eds., Amsterdam, Netherlands: Elsevier, 1978, ch. 3, pp. 37–60.
- [58] Y. A., Çengel and J. M. Cimbala, "Internal Flow: The Entrance region" in *Fluid mechanics: Fundamentals and Applications*, 3rd ed. New York, NY, USA: McGraw-Hill, 2014, ch. 8-3, pp 351-353. [Online]. Available: <https://engineeringbooklibrary.files.wordpress.com/2019/03/fluid-mechanics-fundamentals-and-applications-3rd-edition-cengel-and-cimbala-2014.pdf>
- [59] "La presión arterial alta". National Institute on Aging, US Department of Health & Human Services, Bethesda, Maryland, USA. [Online]. Available: <https://www.nia.nih.gov/espanol/presion-arterial-alta>
- [60] "Presión arterial alta: Qué significa y qué hacer al respecto", National Institutes of Health. US Department of Health & Human Services, Bethesda, Maryland, USA. [Online]. Available: <https://salud.nih.gov/preguntele-a-carla/presion-arterial-alta-que-significa-y-que-hacer-al-respecto>

- [61] "Presión arterial alta (hipertensión arterial)", The Texas Heart Institute, Houston, Texas, USA. [Online]. Available: <https://www.texasheart.org/heart-health/heart-information-center/topics/presion-arterial-alta-hipertension-arterial/>
- [62] P. Shi, S. Hu, Y. Zhu, J. Zheng, Y. Qiu, and P. Y.S. Cheang, "Insight into the dicrotic notch in photoplethysmographic pulses from the finger tip of young adults", *Journal of Medical Engineering & Technology*, vol.33, pp.628-33, Dec. 2009.
- [63] T. OBrien, L. Morris, and T. McGloughlin, "Evidence suggests rigid aortic grafts increase systolic blood pressure: Results of a preliminary study," *Med. Eng. Phys.*, vol. 30, no. 1, pp. 109–115, Jan. 2008.
- [64] "¿Cuánto gana un ingeniero biomédico en España?", Indeed, Austin, Texas, USA, Nov. 4, 2022. [Online]. Available: <https://es.indeed.com/orientacion-laboral/remuneracion-salarios/cuanto-gana-un-ingeniero-biomedico-espana>
- [65] "Taules retributives del personal docent i investigador Any 2022", Universitat Politècnica de Catalunya. BarcelonaTech, Barcelona, Spain. [Online]. Available: [https://www.upc.edu/transparencia/ca/publicitat-activa/informacio-de-personal/20220218 taules retributives del personal docent i investigador any 2022.pdf](https://www.upc.edu/transparencia/ca/publicitat-activa/informacio-de-personal/20220218%20taules%20retributives%20del%20personal%20docent%20i%20investigador%20any%202022.pdf)
- [66] " Taules retributives PDI i PAS", Portal de transparència, Universitat de Barcelona, Barcelona, Spain, Apr. 2023. [Online]. Available : <https://web.ub.edu/es/web/transparencia/tablas-retributivas-pdi-pas>
- [67] "Normes generals reguladores dels treballs de fi de grau de la Universitat de Barcelona", Universitat de Barcelona, Barcelona, Spain, Jun. 5, 2011. [Online]. Available: [https://www.ub.edu/portal/documents/4493882/5180729/normes\\_TFG.pdf/63abc3a2-27ce-8dbd-4463-80e1662ee21d](https://www.ub.edu/portal/documents/4493882/5180729/normes_TFG.pdf/63abc3a2-27ce-8dbd-4463-80e1662ee21d)
- [68] "Normes reguladores dels treballs de fi de grau del grau en Enginyeria Biomèdica", Facultat de Medicina i Ciències de la Salut de Barcelona, Universitat de Barcelona, Barcelona, Spain. [Online]. Available: <https://www.ub.edu/portal/web/medicina-ciencies-salut/graus/-/ensenyament/detallEnsenyament/4917593/10>
- [69] "How to Determine if Your Product is a Medical Device" Center for Devices and Radiological Health & Center for Devices and Radiological Health, U.S. Food and Drug Administration, Sept. 29, 2022. [Online]. Available: <https://www.fda.gov/medical-devices/classify-your-medical-device/how-determine-if-your-product-medical-device>